Supplementary Information (SI) for Chemical Science.

Spontaneous Conversion of Pyridine *N*-Oxide Ylide Covalent Organic Framework (COF) into Biradical COF as an Efficient Catalyst in Catalytic Dehydrogenation of Nitrogen Heterocycles

Wenying Ai[‡*ab], Jiawei Zou[‡a], Zhenfeng Cao[a], Kun Cui[c], Jianbing Gu[a], Lina Du[d], Xin Peng[d], Mingli Jiao[*a], Tao Shen[*c], Lingbo Qu[*b]

[a] School of Materials Electronics and Energy Storage, Zhongyuan University of Technology, Zhengzhou, Henan 450007, P. R. China.

[b] College of Chemistry and Institute of Green Catalysis, Zhengzhou University, Zhengzhou, Henan Province 450001, People's Republic of China.

[c] Frontiers Science Center for Transformative Molecules, School of Chemistry and Chemical Engineering, Zhangjiang Institute for Advanced Study, Shanghai Jiao Tong University, Shanghai, 200240, P. R. China.

[d] Henan Key Laboratory of Nanocomposites and Applications, Institute of Nanostructured Functional Materials, Huanghe Science and Technology College, Zhengzhou 450006, China.

Contents

Section A. Materials and Methods

Section B. Synthetic Procedures

Section C. Supporting Figures

Section D. Supporting Tables

Section E. ^{1}H NMR Spectra

Section F. Copies of NMR Spectra

Section G. Supporting References

Section A. Materials and Methods

Nuclear magnetic resonance spectra (^{1}H NMR and ^{13}C NMR) were measured on a Bruker 400 MHz spectrometer. The chemical shifts were reported in ppm referenced to the deuterated solvents. Solid state Fourier ^{13}C NMR spectra were measured on a Bruker 400 MHz spectrometer. X-ray diffraction (XRD) data were performed on a Bruker D8 Focus Powder X-ray Diffractometer by using powder on glass substrate, from $2\theta = 2°$ up to 30° with 0.01° increment. Fourier transform infrared (FT IR) spectra were recorded on a JASCO model FT IR-6100 infrared spectrometer. TGA measurements were recorded on a Discovery TGA under N_2, by heating from 30 to 800 °C at a rate of 10 °C min^{-1}. Elemental analysis was performed on an Elementar vario MICRO cube elemental analyzer. Nitrogen sorption isotherms were measured at 77 K with a TriStar II instrument (Micromeritics). The Brunauer-Emmett-Teller (BET) method was utilized to calculate the specific surface areas. By using the non-local density functional theory (NLDFT) model, the pore volume was derived from the sorption curve. Morphology images were characterized with a Zeiss Merlin Compact filed emission scanning electron microscope (FE-SEM) equipped with an energy-dispersive X-ray spectroscopy (EDS) system at an electric voltage of 5 KV. ICP-MS was carried out on a Perkin-Elmer Elan DRC II quadrupole inductively coupled plasma mass spectrometer analyzer. X-ray photoelectron spectroscopy (XPS) experiments were performed on a Thermo Scientific K-Alpha XPS spectrometer using an AlKa X-ray radiation source.

Section B. Synthetic Procedures

2,6-Pyridine dialdehyde, 1,3,5-tris(4-aminophenyl)benzene, AcOH, aniline, *n*-Butanol (*n*-BuOH) and 1,2-dichlorobenzene (*o*-DCB) were purchased from Heowns. All the other solvents were purchased from Heowns and used as received without further purification.

Synthesis of 2,6-Bis[(phenylimine) methyl] pyridine

2,6-Bis[(phenylimine) methyl] pyridine should be prepared referring the synthetic method reported by Nunes, Fábio Souza's group in 2022[1]. Aniline (740 μL, 7.85mmol) and 2,6-pyridine dialdehyde (505mg, 3.74mmol) were dissolved in EtOH (60 mL) and stirred at 85°C for 24 h. After evaporation of the solvent, the resulting solid was dissolved in 25 mL of CH_2Cl_2, and the solution was washed with water. The organic phase was separated, dried with anhydrous $MgSO_4$ and concentrated under vacuum, resulting in target product as a brown powder. The crude product was used directly in next step without further purification.

Synthesis of 2-formyl-6-(phenylcarbamoyl)pyridine 1-oxide

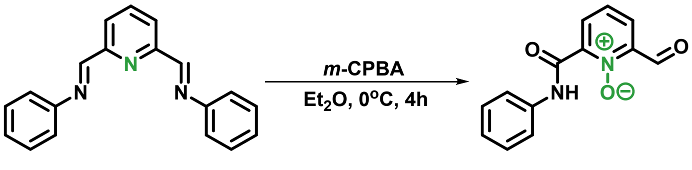

To the solution of 2,6-bis[(phenylimine) methyl] pyridine (100 mg, 0.35mmol) in diethyl ether (10 mL) was added *m*-CPBA (181.6 mg, 1.05 mmol) at 0 °C. Then the mixture was stirred at 0 °C for 4 hours. After the start material disappearing, the reaction was quenched by saturated sodium carbonate solution. And the resulting mixture was extracted with Et_2O. The organic layer was dried over anhydrous magnesium sulfate, and the solvent was removed under reduced pressure. The residue was purified by column chromatography (EtOAc/petroleum ether) to obtain the desired product. **^{1}H NMR (400 MHz, $CDCl_3$)** δ 10.18 (s, 1H), 9.93 (s, 1H), 8.56 (dd, *J* = 7.0, 1.8 Hz, 1H), 8.17 – 8.12 (m, 2H), 7.81 (d, *J* = 7.8 Hz, 2H), 7.42 (t, *J* = 7.9 Hz, 2H), 7.19 (d, *J* = 7.5 Hz, 1H). **^{13}C NMR (100 MHz, $CDCl_3$)** δ 192.09, 160.89, 139.11, 137.32, 130.28, 129.22, 126.68, 124.82, 124.10, 119.93. **HRMS m/z (ESI)** calcd for C13H11N2O3+ (M + H) + 243.0764, found 243.0757.

Synthesis of Bipy-COF. The synthesis of **Bipy-COF** was carried out via Schiff-base condensation of 2,6-pyridine dialdehyde **1** (30.4 mg, 0.225 mmol) and 1,3,5-tris(4-aminophenyl)benzene **2** (52.6 mg, 0.15 mmol) in *o*-DCB : *n*-butanol (1.5mL, 1:1) using 6 M AcOH aqueous (0.15 mL). Then the suspension was sonicated and heated at 120 °C for 3 days using glass ampule. The resulting precipitate was washed with THF (3×10 mL) and MeOH (3×10 mL) and dried under vacuum overnight to generate **Bipy-COF** as a tawny powder in 93% yield.

Synthesis of DICPO-COF. Bipy-COF (100 mg, 0.3 mmol) was added to 20 mL of diethyl ether (Et_2O), followed by the slow addition of m-CPBA (103.6 mg, 0.6 mmol). The mixture was stirred at 0 °C for 4 hours. Upon completion of the reaction, the mixture was quenched with 5% Na_2SO_4 solution, and the solid product was washed with water and then collected by filtration. The resulting solid was dried under vacuum at 60 °C for 4 hours to yield **DICPO-COF** in 98% yield.

General Procedure for the Optimization of Reaction Conditions for the DICPO-COF-catalyzed Dehydrogenation of Tetrahydroquinoline.

In a 10 mL reaction vial, **DICPO-COF** (5 mg), $CuCl_2$ (1 mg), and H_2O (0.5 mL) were sequentially added, followed by the addition of 1,2,3,4-tetrahydroquinoline (5 μL). The mixture was stirred at 85 °C for 22 hours. After completion of the reaction, the mixture was cooled to room temperature and extracted with ethyl acetate (EtOAc). The organic layer was washed with saturated brine, dried over anhydrous Na_2SO_4, and the solvent was removed under vacuum. The crude product was purified by column chromatography (petroleum ether/EtOAc) to afford quinoline.

General Procedure for the Dehydrogenation of Tetrahydroquinolines and Indolines.

In a 100 mL reaction vial, **DICPO-COF** (50 mg), $CuCl_2$ (5 mg, 0.03719 mmol, 10 mol%.), and H_2O (5 mL) were sequentially added, followed by the addition of tetrahydroquinoline or indolines (0.4 mmol, 1 eq.). The mixture was stirred at 85 °C for 22 hours. After tetrahydroquinoline or indolines disappearing, the mixture was cooled to room temperature and extracted with ethyl acetate (EtOAc). The organic layer was washed with saturated brine, dried over anhydrous Na_2SO_4, and the solvent was removed under vacuum. The crude product was purified by column chromatography (petroleum ether/EtOAc) to afford quinoline (52-85%).

Section C. Supporting Figures

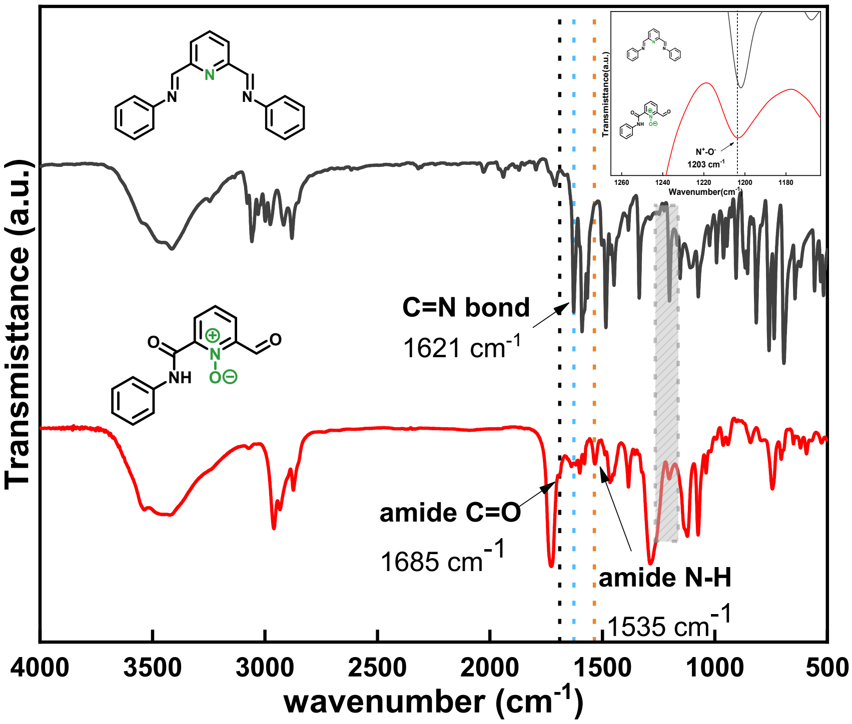

Figure S1. FT-IR spectra of 2,6-Bis[(phenylimine) methyl] pyridine (grey line) and 2-formyl-6-(phenylcarbamoyl)pyridine 1-oxide (red line).

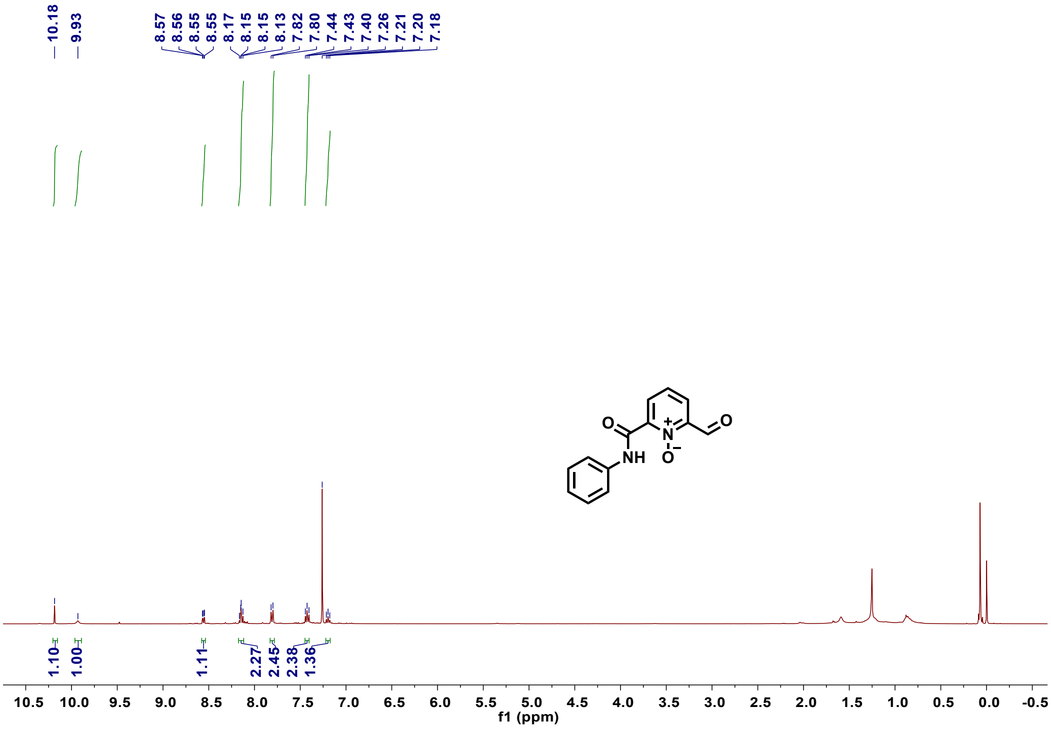

Figure S2. The experimental ^{1}H NMR spectra of 2,6-Bis[(phenylimine) methyl] pyridine.

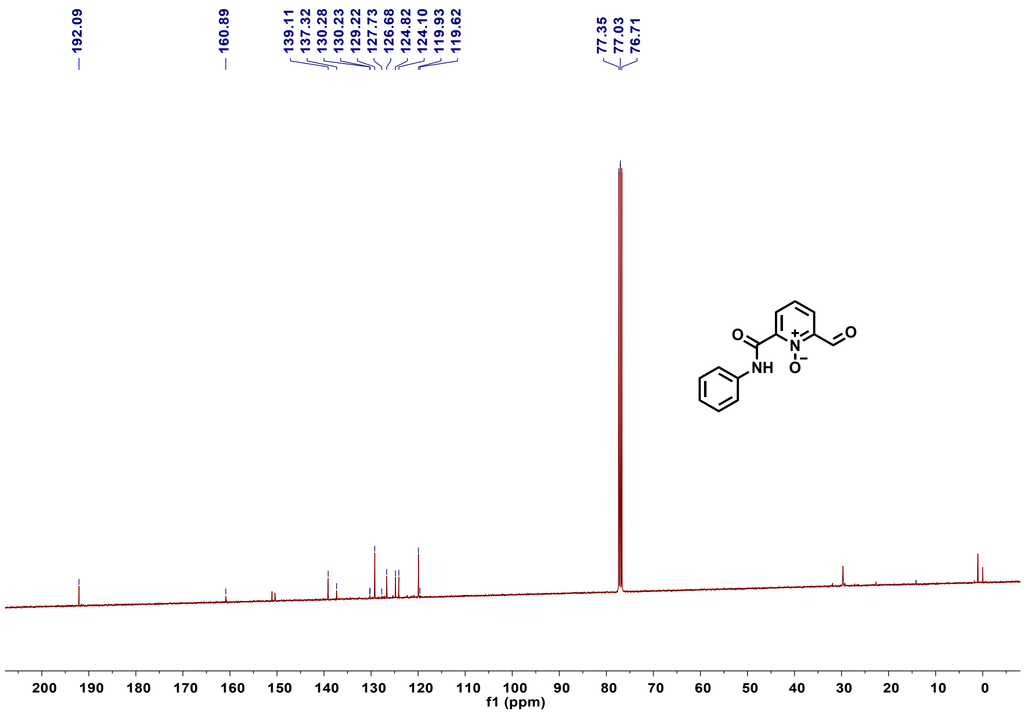

Figure S3. The experimental ^{13}C NMR spectra of 2,6-Bis[(phenylimine) methyl] pyridine.

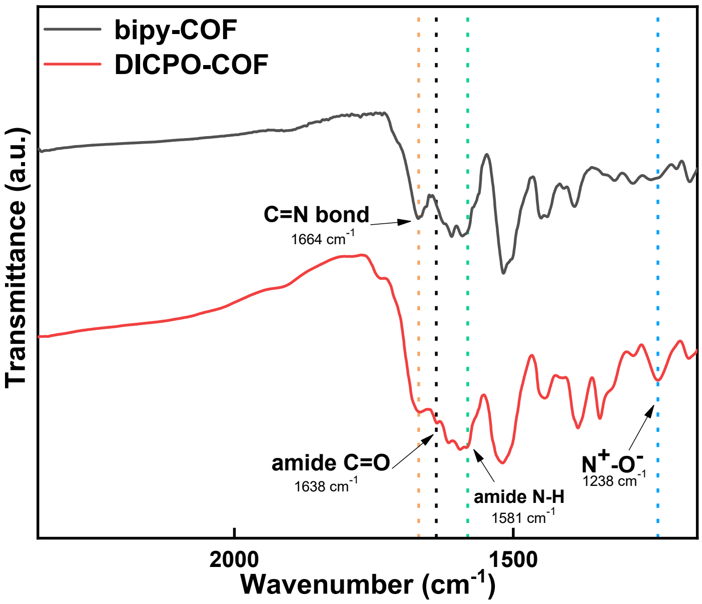

Figure S4. FT-IR spectra of **Bipy-COF (**grey line**)** and **DICPO-COF (**green line**)**.

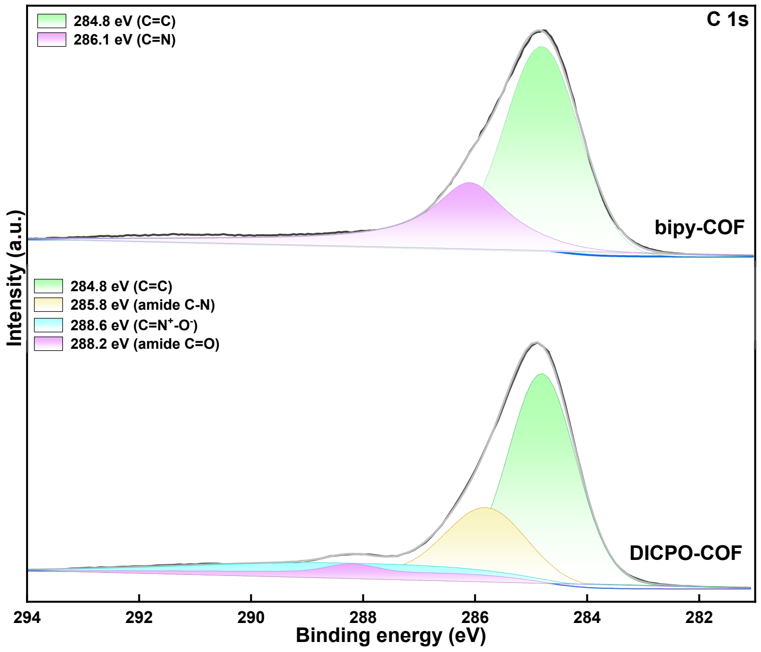

Figure S5. C 1s XPS spectra of **Bipy-COF** and **DICPO-COF**.

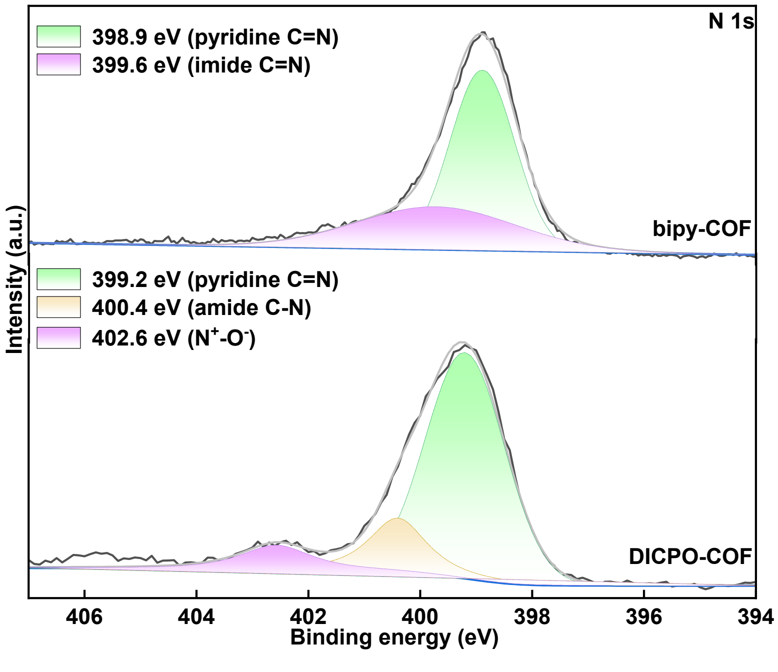

Figure S6. N 1s XPS spectra of **Bipy-COF** and **DICPO-COF**.

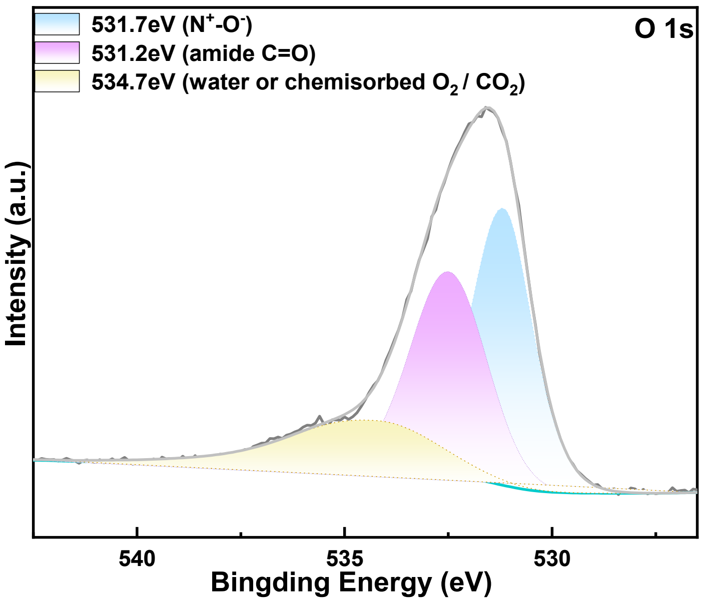

Figure S7. O 1s XPS spectra of **DICPO-COF**.

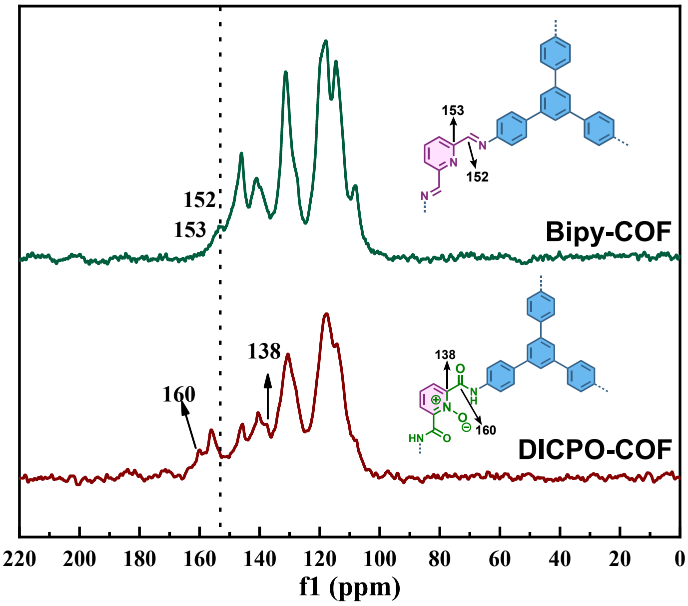

Figure S8. The 13C CP/MAS NMR spectrum of **Bipy-COF** and **DICPO-COF.**

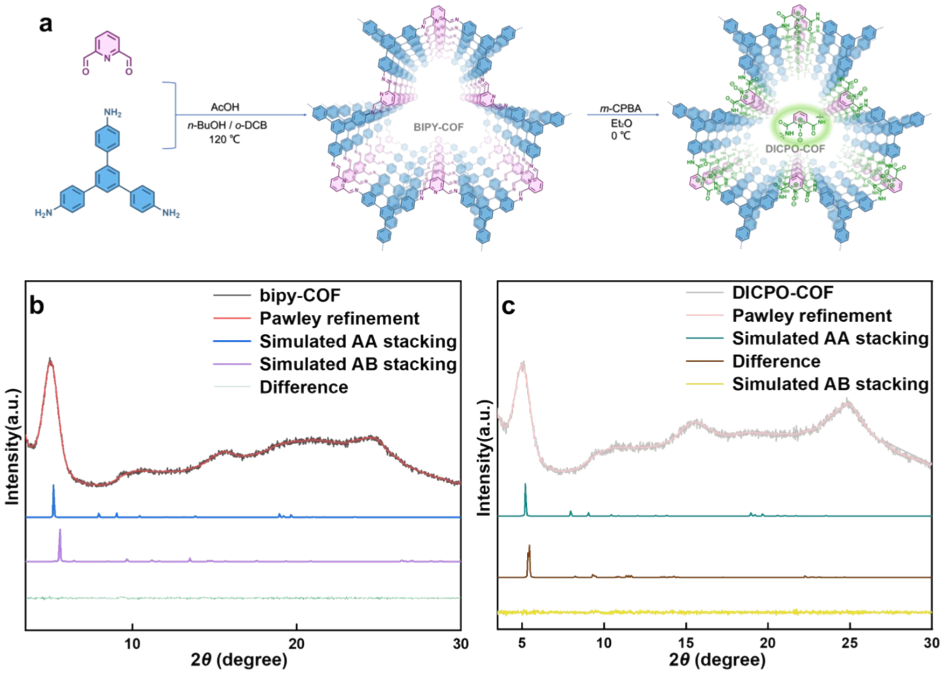

Figure S9. (a) Synthesis of **Bipy-COF** from **DICPO-COF**. (b) Experimentally observed PXRD patterns of **Bipy-COF** (red), simulated curves for AA-stacking mode (grey line), and AB-stacking mode (blue line). (c) Experimentally observed PXRD patterns of **DICPO-COF** (blue line), simulated curves for AA-stacking mode (grey line), and AB-stacking mode (red line). (d) Experimental PXRD patterns of **Bipy-COF** (grey line) and **DICPO-COF** (red line).

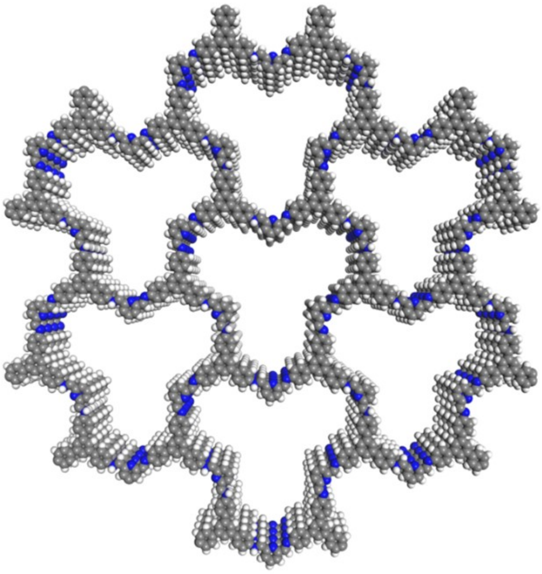

Figure S10. Top views of the AA-stacking mode of **Bipy-COF** (seven units).

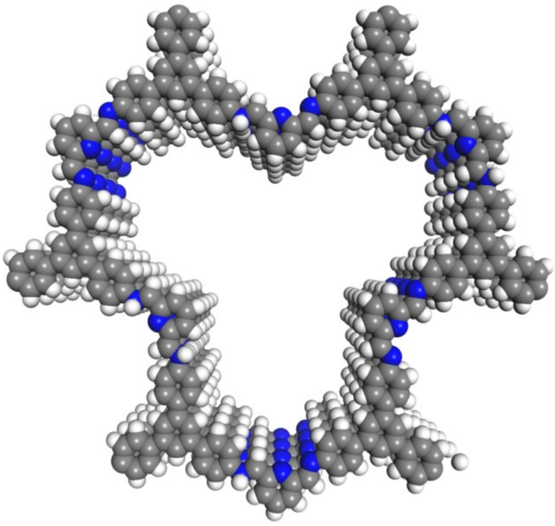

Figure S11. Top views of the AA-stacking mode of **Bipy-COF** (one unit).

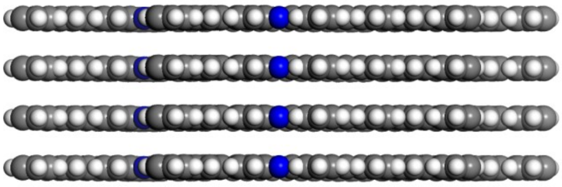

Figure S12. Side views of the AA-stacking mode of **Bipy-COF**.

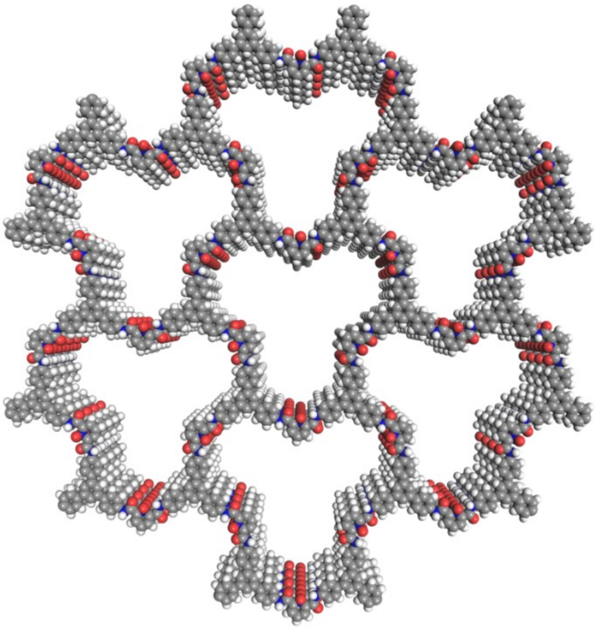

Figure S13. Top views of the AA-stacking mode of **DICPO-COF** (seven units).

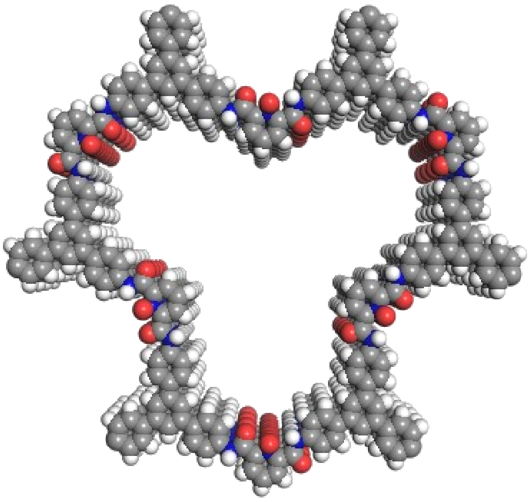

Figure S14. Top views of the AA-stacking mode of **DICPO-COF** (one units).

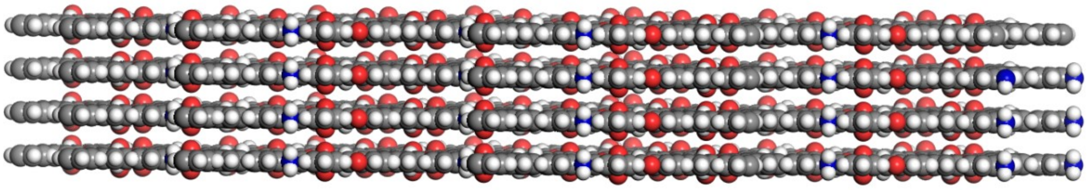

Figure S15. Side views of the AA-stacking mode of **DICPO-COF**.

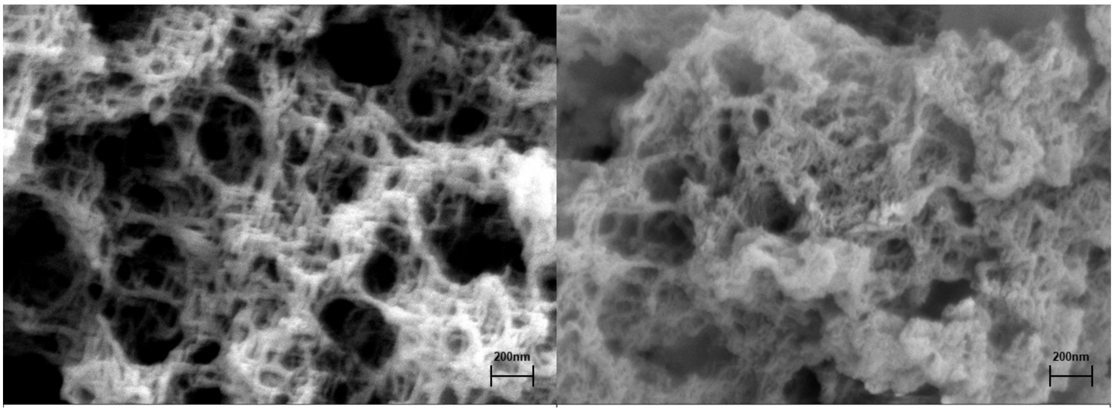

Figure S16. SEM images of **Bipy-COF** (a) and **DICPO-COF** (b)**;**

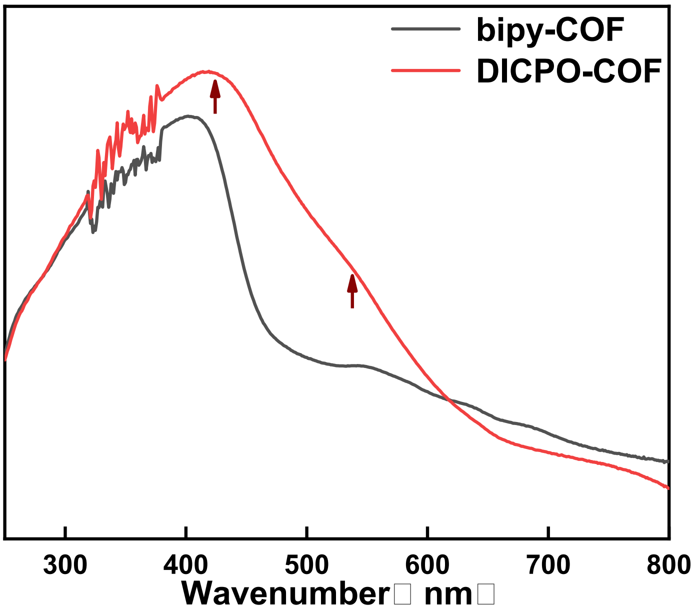

Figure S17. The solid-state UV-vis spectra of **Bipy-COF** (black) and **DICPO-COF** (red).

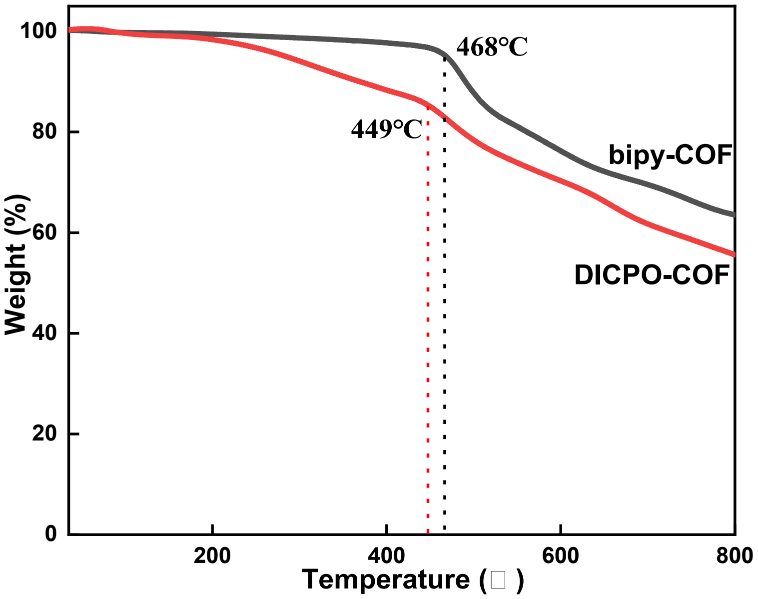

Figure S18. Thermogravimetric curves of **Bipy-COF** (black) and **DICPO-COF** (red).

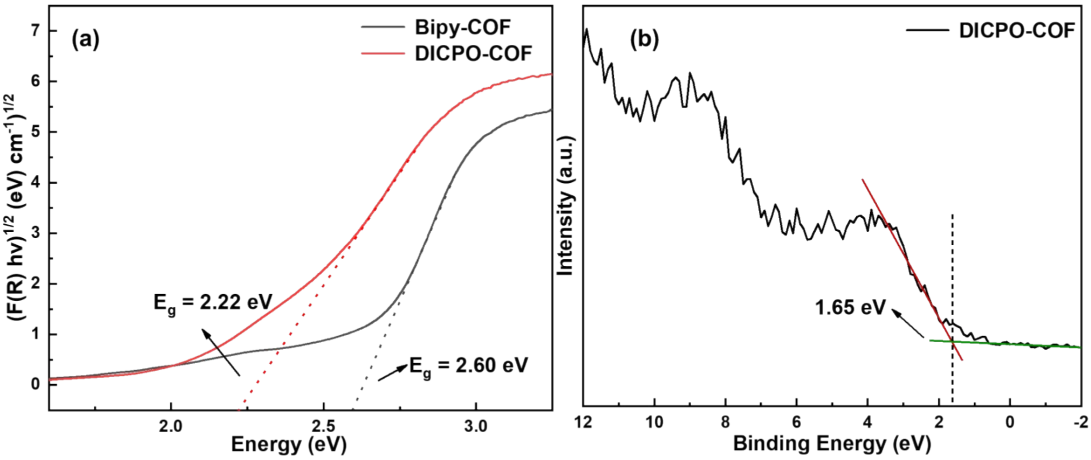

Figure S19. (a)The optical bandgap of **Bipy-COF** (black) and **DICPO-COF** (red) evaluated from the Kubelka–Munk function; (b) VB XPS spectrum of **DICPO-COF.**

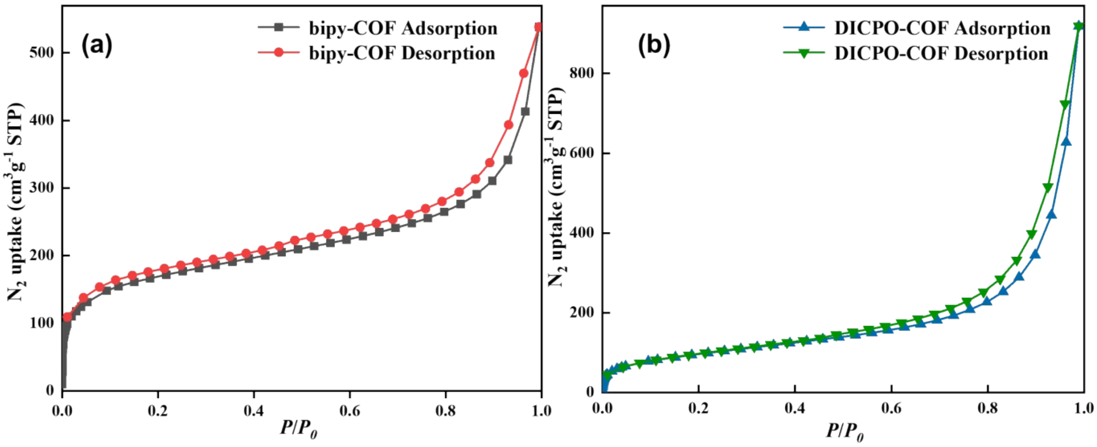

Figure S20. Nitrogen adsorption–desorptionisotherms of **Bipy-COF** and **DICPO-COF**.

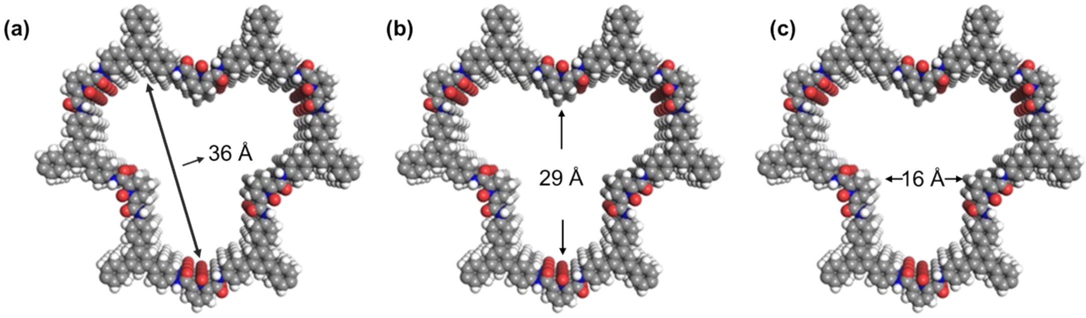

Figure S21. Simulated pore size distribution.

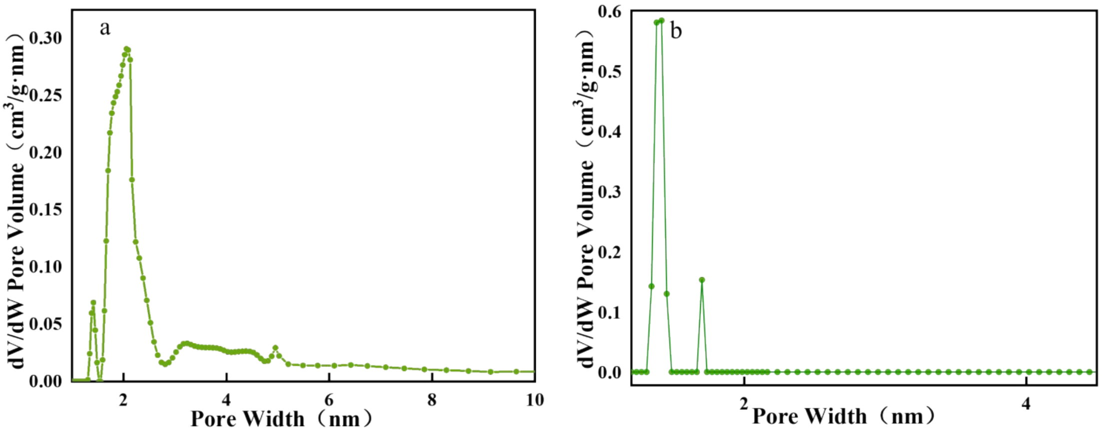

Figure S22. Pore size distribution profiles of **Bipy-COF** (a) and **DICPO-COF** (b) through nitrogen adsorption-desorption isotherms.

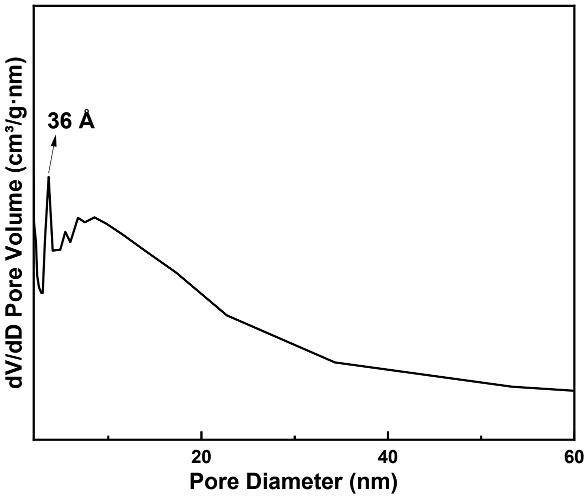

Figure S23. The argon adsorption analyses of **DICPO-COF**.

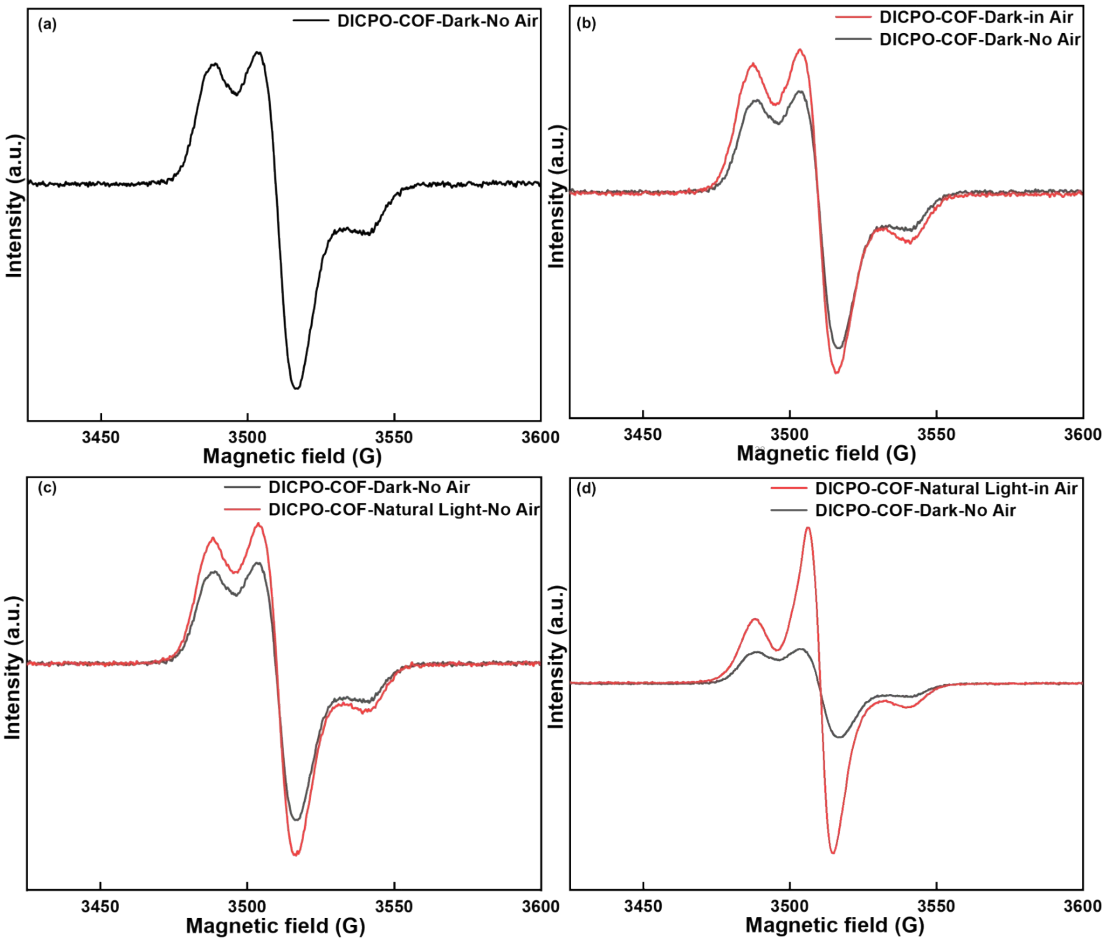

Figure S24. EPR spectra of **DICPO-COF** in the dark and without air (a), in the dark and with air (b), under the natural light without air (c) and under the natural light with air (d).

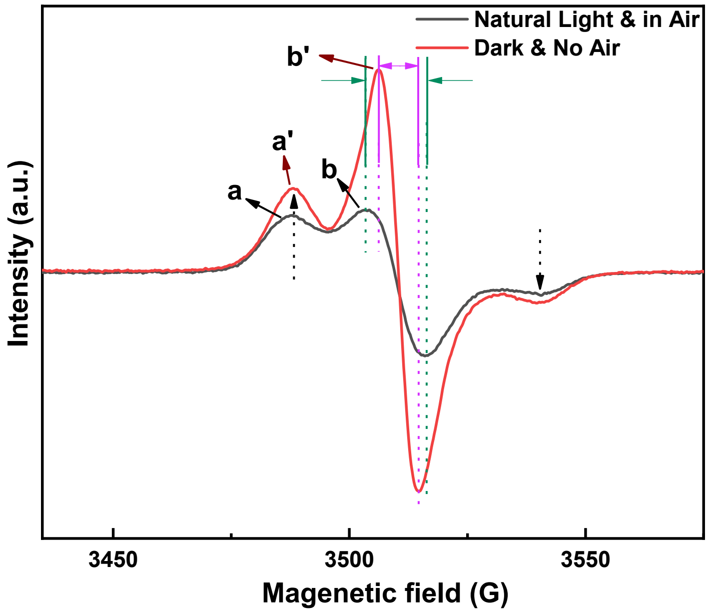

Figure S25. EPR spectra of **DICPO-COF** in the dark and without air and under the natural light with air.

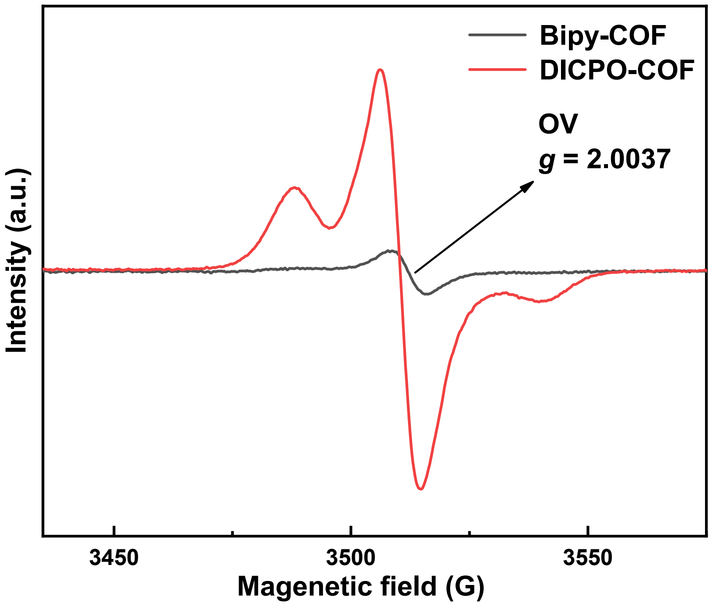

Figure S26. EPR of **Bipy-COF** and **DICPO-COF.**

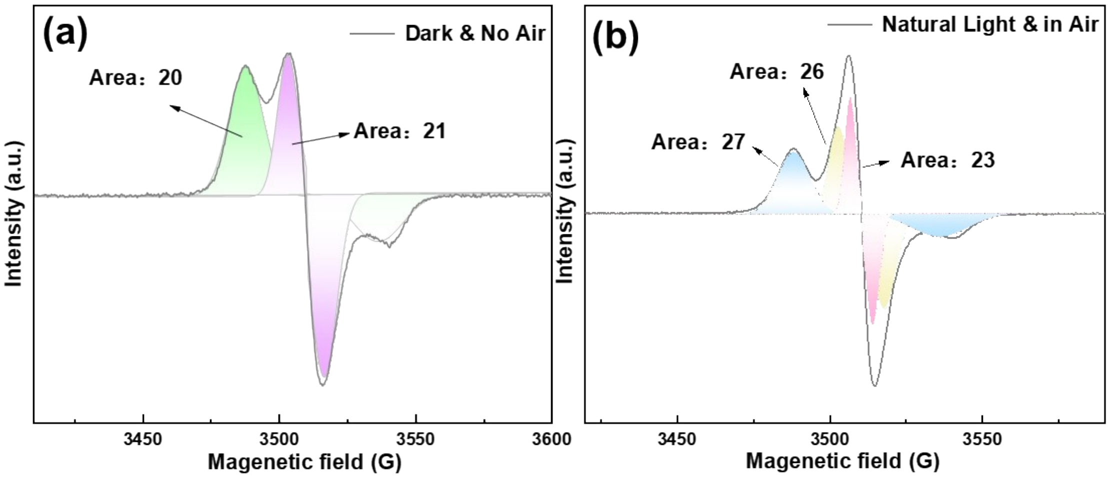

Figure S27. EPR spectral analysis (peak fitting and quantification) of **DICPO-COF** under (a) dark/air-free and (b) natural light/air conditions.

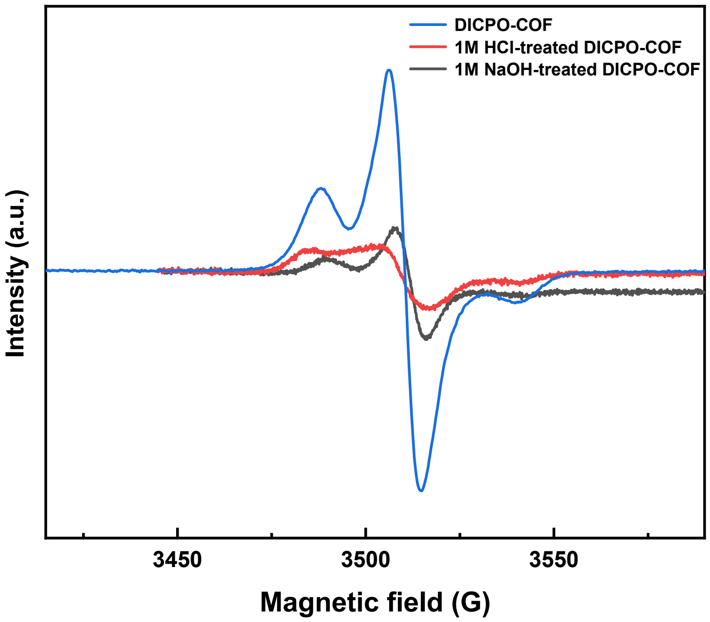

Figure S28. EPR spectra of **DICPO-COF** after treatment under HCl (1 M, red) and NaOH (1M, black) at room temperature.

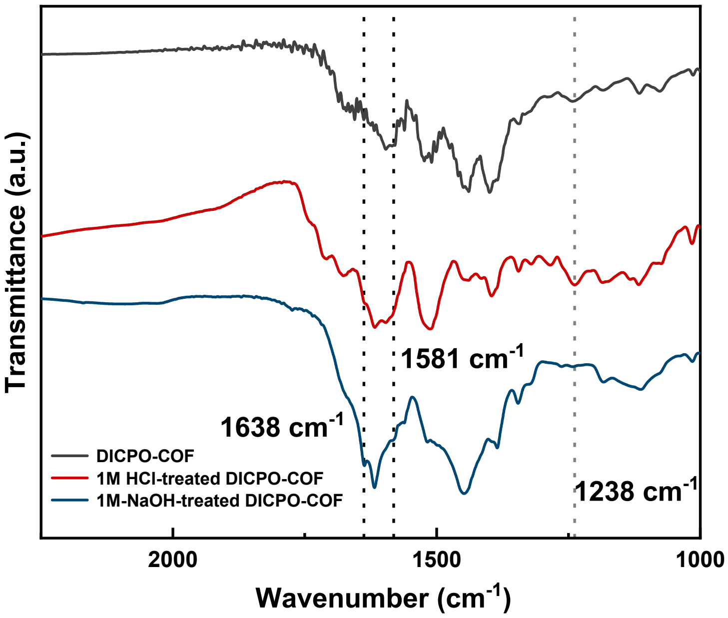

Figure S29. FT-IR spectra of **DICPO-COF** after treatment under HCl (1 M, red) and NaOH (1M, blue) at room temperature.

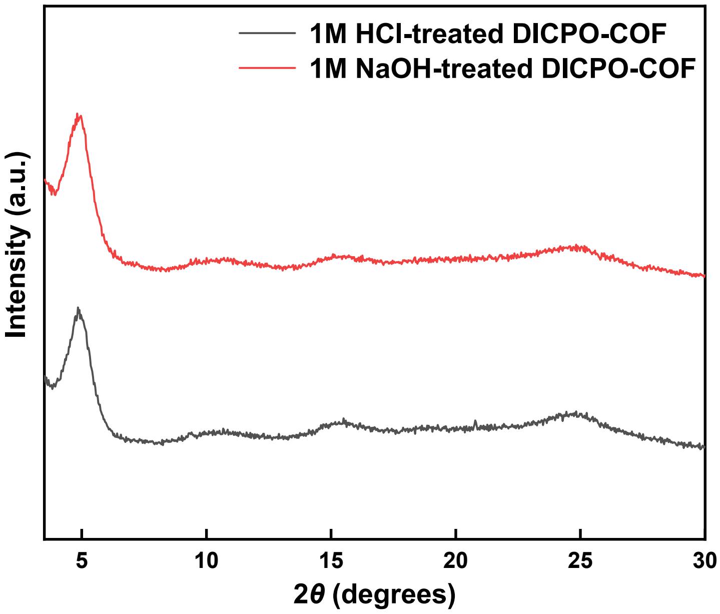

Figure S30. PXRD patterns of **DICPO-COF** after after acid (1 M HCl, black) or base (1 M NaOH, red) treatment.

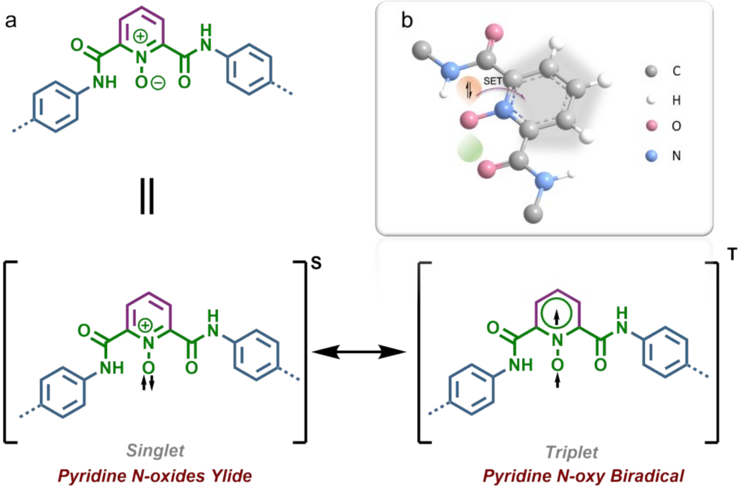

Figure S31. (a) Schematic illustration of the SET (single electron transfer) pathway of the pyridine N-oxide ylide COF (**DICPO-COF**); b) The proposed electronic configurations of **DICPO-COF** are displayed in brackets as two resonance structures.

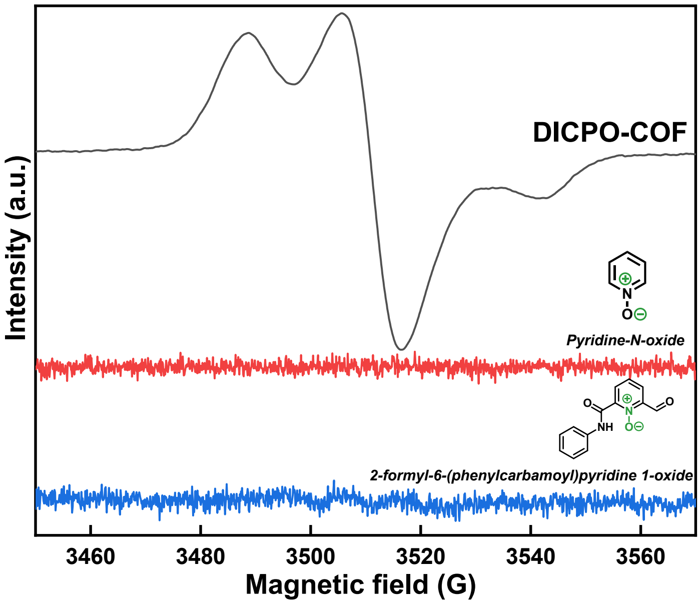

Figure S32. EPR spectra of **DICPO-COF**, Pyridine-*N*-oxide and small molecule form (2-formyl-6-(phenylcarbamoyl)pyridine 1-oxide).

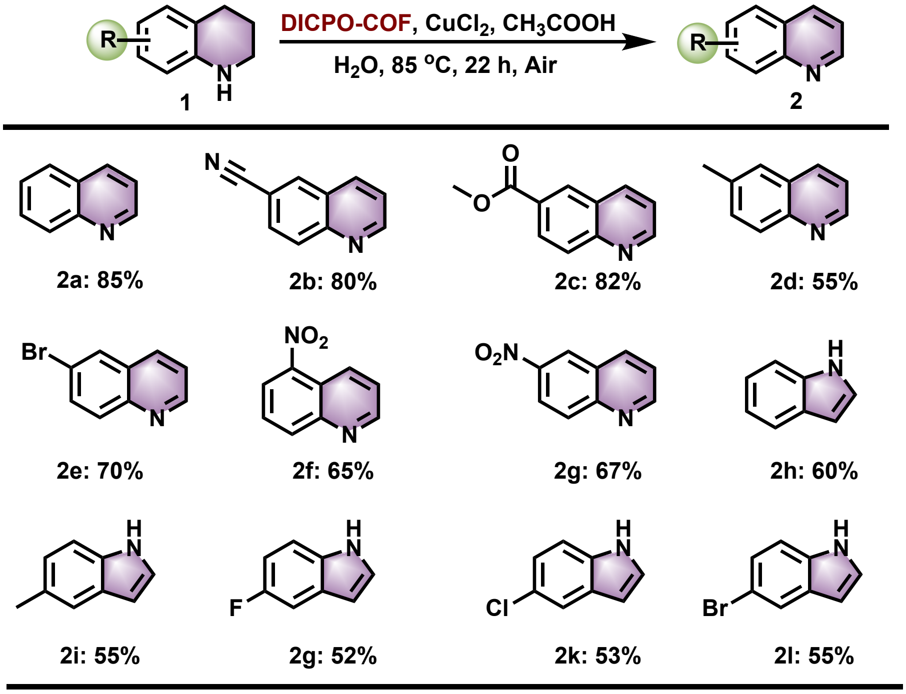

Figure S33. Scope of the dehydrogenation of tetrahydroquinolines and indolines.

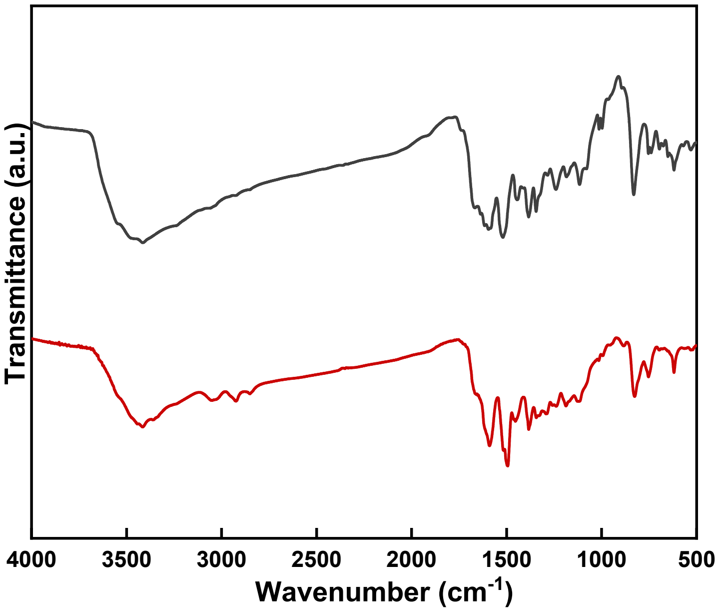

Figure S34. The FT-IR spectra of **DICPO-COF** before (black) and after the fifth cycle (red) in the gram scale reaction.

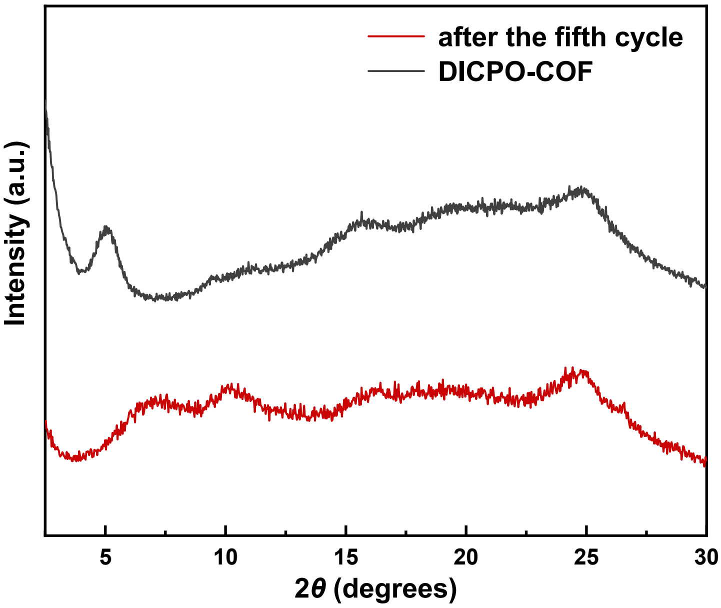

Figure S35. Experimental PXRD patterns of **DICPO-COF** (black) and after the fifth cycle (red).

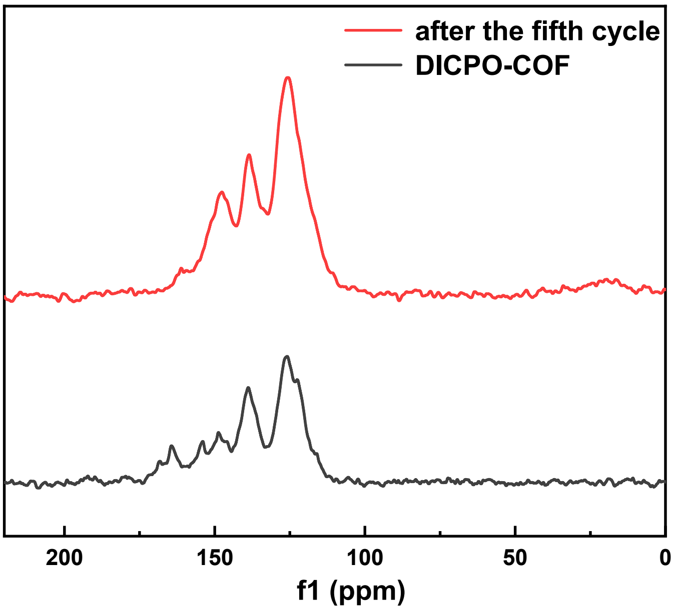

Figure S36. The ^{13}C CP/MAS NMR spectrum of **DICPO-COF** (black) and after the fifth cycle (red)

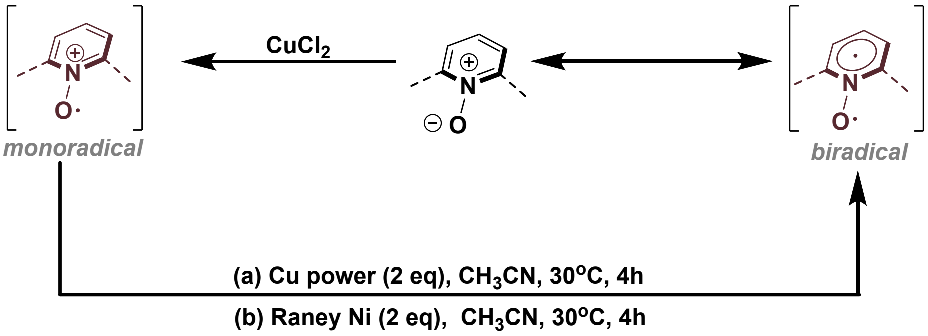

Figure S37. Using Cu powder and Raney Ni as reducing agents to react with the monoradical species generated after the catalytic reaction.

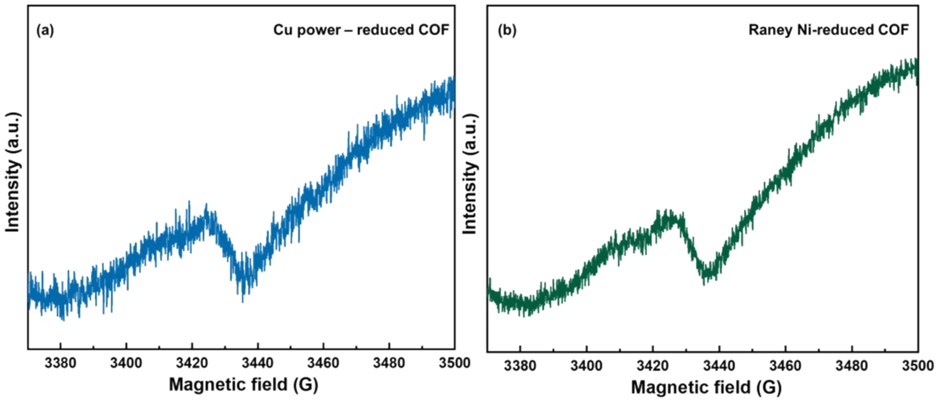

Figure S38. (a) EPR spectrum of the Cu power-reduced COF. (b) EPR spectrum of the Raney Ni-reduced COF.

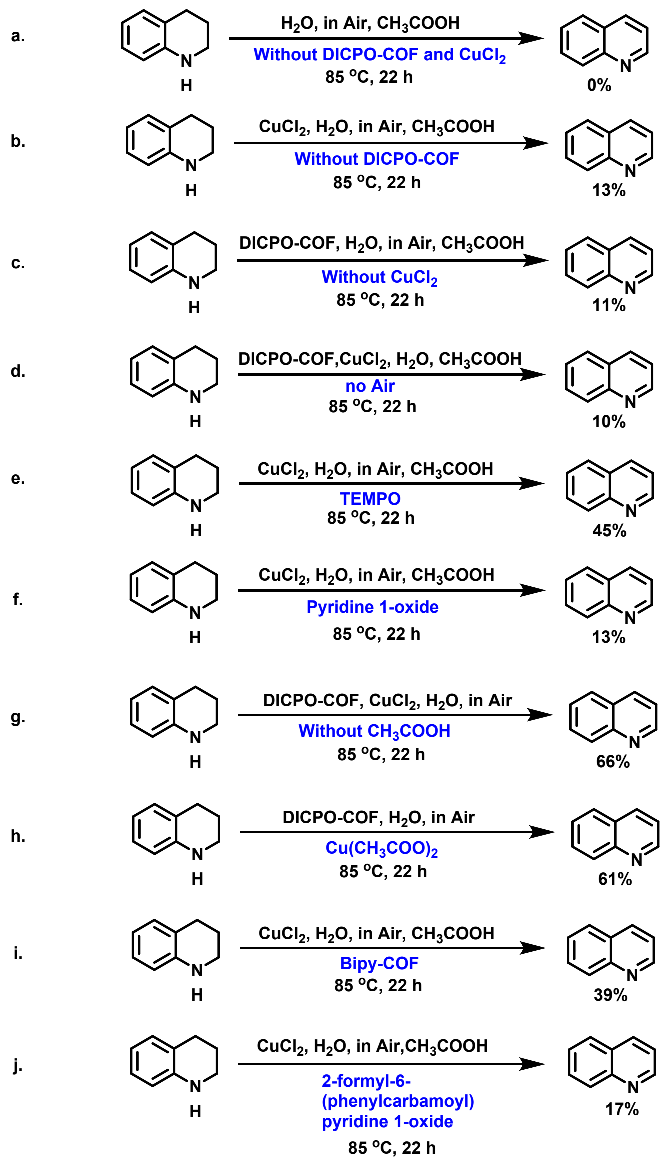

Figure S39. Control experiments.

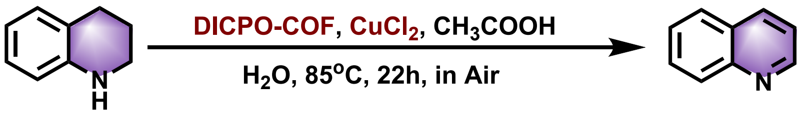

entry	N-heterocyclic substrate	DICPO-COF	$CuCl_2$	yield
1	50 uL, 0.40 mmol, 1 eq	50 mg	10 mg, 0.07 mmol, 19 mol%	86%
2	50 uL, 0.40 mmol, 1 eq	50 mg	20 mg, 0.14mmol, 38 mol%	85%
3	50 uL, 0.40 mmol, 1 eq	100 mg	10 mg, 0.07 mmol, 19 mol%	88%

Figure S40. Under standard conditions with double the original amount of both $CuCl_2$ and **DICPO-COF.**

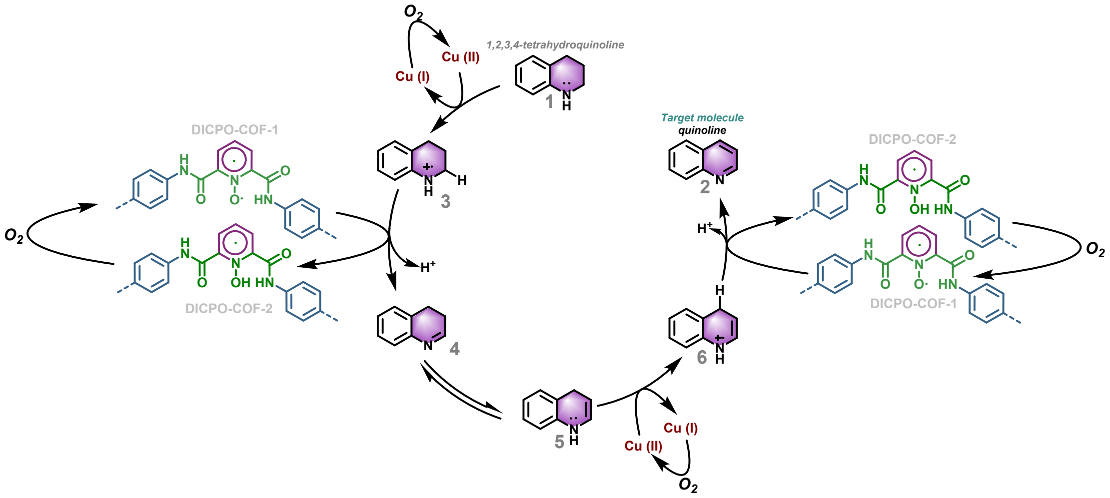

Figure S41. Proposed mechanism.

Section D. Supporting Tables

Table S1. Dehydrogenation of 1,2,3,4-Tetrahydroquinoline. Conditions: 1,2,3,4-Tetrahydroquinoline (0.03754 mmol, 1.0 equiv), [Cu] (5 mg), solvent (0.5 mL), 85°C, 22h.

entry	solvent	catalyst	temperature	metal	yield
1	MeOH	none	60°C	none	none
2	MeOH	none	60°C	$CuCl_2$	20%
3	MeOH	bipy-COF	60°C	$CuCl_2$	35%
4	MeOH	DICPO-COF	60°C	$CuCl_2$	50%
5	THF	DICPO-COF	60°C	$CuCl_2$	30%
6	EtOH	DICPO-COF	60°C	$CuCl_2$	55%
7	hexane	DICPO-COF	60°C	$CuCl_2$	45%
8	H_2O	DICPO-COF	60°C	$CuCl_2$	70%
9	H_2O	DICPO-COF	60°C	$Cu(OAc)_2$	65%
10	H_2O	DICPO-COF	60°C	$NiCl_2$	68%
11	H_2O	DICPO-COF	60°C	$Ni(OAc)_2$	62%
12	H_2O	DICPO-COF	60°C	$FeCl_3$	65%
13	H_2O	DICPO-COF	60°C	$FeCl_2$	67%
14	H_2O	DICPO-COF	60°C	$CoCl_2$	71%
15	H_2O	DICPO-COF	60°C	$Co(OAc)_2$	67%
16	H_2O	DICPO-COF	70°C	$CuCl_2$	72%
17	H_2O	DICPO-COF	80°C	$CuCl_2$	81%
18	H_2O	DICPO-COF	90°C	$CuCl_2$	78%
19	H_2O	DICPO-COF	85°C	$CuCl_2$	85%

Table S2. Atomistic coordinates for the AA-stacking mode of **Bipy-COF** optimized using DFTB+ method. Space group: P6; α = β = 90°, γ = 120°, a = 33.9273 Å, b = 33.8870 Å, c = 4.6811 Å.

C1	C	0.36214	0.7444	0.5	0	1
C2	C	0.36319	0.70087	0.5	0	1
C3	C	0.40652	0.7006	0.5	0	1
C4	C	0.45059	0.74326	0.5	0	1
C5	C	0.4508	0.78689	0.5	0	1
C6	C	0.40753	0.78745	0.5	0	1
N7	N	0.49371	0.74012	0.5	0	1
C8	C	0.53798	0.77532	0.5	0	1
C9	C	0.31481	0.74484	0.5	0	1
C10	C	0.26994	0.70181	0.5	0	1
C11	C	0.22551	0.70082	0.5	0	1
C12	C	0.22724	0.74546	0.5	0	1
C13	C	0.27084	0.78982	0.5	0	1
C14	C	0.31399	0.78823	0.5	0	1
C15	C	0.27129	0.83744	0.5	0	1
C16	C	0.17766	0.65351	0.5	0	1
C17	C	0.22807	0.83936	0.5	0	1
C18	C	0.22852	0.88296	0.5	0	1

C19	C	0.27223	0.92666	0.5	0	1
C20	C	0.3151	0.92568	0.5	0	1
C21	C	0.31493	0.88224	0.5	0	1
C22	C	0.1756	0.60844	0.5	0	1
C23	C	0.1318	0.56517	0.5	0	1
C24	C	0.08801	0.56496	0.5	0	1
C25	C	0.08911	0.60874	0.5	0	1
C26	C	0.13276	0.65213	0.5	0	1
N27	N	0.27514	0.97272	0.5	0	1
C28	C	0.23947	0.98102	0.5	0	1
N29	N	0.04174	0.52168	0.5	0	1
C30	C	0.0333	0.47775	0.5	0	1
C31	C	0.57758	0.7649	0.5	0	1
N32	N	0.56762	0.71854	0.5	0	1
C33	C	0.60279	0.7067	0.5	0	1
C34	C	0.65127	0.74335	0.5	0	1
C35	C	0.66243	0.7912	0.5	0	1
C36	C	0.62558	0.80224	0.5	0	1
C37	C	0.58878	0.65561	0.5	0	1
N38	N	0.62292	0.64247	0.5	0	1
C39	C	0.61709	0.59754	0.5	0	1
C40	C	0.65838	0.59357	0.5	0	1

C41	C	0.65531	0.54875	0.5	0	1
C42	C	0.61023	0.50543	0.5	0	1
C43	C	0.56868	0.51029	0.5	0	1
C44	C	0.57197	0.55521	0.5	0	1
C45	C	0.60658	0.45631	0.5	0	1
C46	C	0.64806	0.45174	0.5	0	1
C47	C	0.64589	0.40687	0.5	0	1
C48	C	0.59968	0.36546	0.5	0	1
C49	C	0.55679	0.36749	0.5	0	1
C50	C	0.56154	0.41347	0.5	0	1
C51	C	0.69151	0.40324	0.5	0	1
C52	C	0.68962	0.35826	0.5	0	1
C53	C	0.73143	0.35512	0.5	0	1
C54	C	0.77681	0.39623	0.5	0	1
C55	C	0.77987	0.44122	0.5	0	1
C56	C	0.73816	0.44465	0.5	0	1
C57	C	0.50739	0.32194	0.5	0	1
C58	C	0.5022	0.27549	0.5	0	1
C59	C	0.45693	0.23385	0.5	0	1
C60	C	0.4148	0.23678	0.5	0	1
C61	C	0.419	0.28195	0.5	0	1
C62	C	0.46408	0.32369	0.5	0	1

N63	N	0.36717	0.19539	0.5	0	1
N64	N	0.81827	0.39021	0.5	0	1
C65	C	0.86329	0.42377	0.5	0	1
C66	C	0.90175	0.41159	0.5	0	1
C67	C	0.35575	0.15055	0.5	0	1
C68	C	0.30493	0.11213	0.5	0	1
C69	C	0.26719	0.12227	0.5	0	1
C70	C	0.21965	0.08448	0.5	0	1
C71	C	0.20995	0.03713	0.5	0	1
C72	C	0.24833	0.02803	0.5	0	1
C73	N	0.29446	0.06562	0.5	0	1
C74	C	0.89147	0.36376	0.5	0	1
C75	C	0.92931	0.35422	0.5	0	1
C76	C	0.97685	0.39202	0.5	0	1
C77	C	0.9861	0.43945	0.5	0	1
N78	N	0.94845	0.44779	0.5	0	1
H79	H	0.33137	0.66598	0.5	0	1
H80	H	0.40572	0.66657	0.5	0	1
H81	H	0.48399	0.82094	0.5	0	1
H82	H	0.4114	0.82258	0.5	0	1
H83	H	0.54657	0.81232	0.5	0	1
H84	H	0.26958	0.66877	0.5	0	1

H85	H	0.19435	0.74566	0.5	0	1
H86	H	0.34721	0.82104	0.5	0	1
H87	H	0.19283	0.80795	0.5	0	1
H88	H	0.19426	0.88162	0.5	0	1
H89	H	0.34921	0.95908	0.5	0	1
H90	H	0.34993	0.88554	0.5	0	1
H91	H	0.20705	0.60476	0.5	0	1
H92	H	0.13305	0.53232	0.5	0	1
H93	H	0.05564	0.60927	0.5	0	1
H94	H	0.12953	0.68375	0.5	0	1
H95	H	0.20255	0.95195	0.5	0	1
H96	H	0.06241	0.47007	0.5	0	1
H97	H	0.68013	0.73521	0.5	0	1
H98	H	0.69968	0.81975	0.5	0	1
H99	H	0.6344	0.8394	0.5	0	1
H101	H	0.69359	0.6257	0.5	0	1
H102	H	0.68929	0.54981	0.5	0	1
H103	H	0.53258	0.48023	0.5	0	1
H104	H	0.53858	0.55556	0.5	0	1
H105	H	0.68231	0.48338	0.5	0	1
H106	H	0.59706	0.33135	0.5	0	1
H107	H	0.52987	0.41591	0.5	0	1

H108	H	0.65657	0.32439	0.5	0	1
H109	H	0.7284	0.32007	0.5	0	1
H110	H	0.81414	0.47418	0.5	0	1
H111	H	0.74426	0.48064	0.5	0	1
H112	H	0.53224	0.26949	0.5	0	1
H113	H	0.45569	0.19975	0.5	0	1
H114	H	0.38683	0.28489	0.5	0	1
H115	H	0.46318	0.35658	0.5	0	1
H116	H	0.87382	0.46131	0.5	0	1
H117	H	0.3829	0.14014	0.5	0	1
H118	H	0.27428	0.15887	0.5	0	1
H119	H	0.1903	0.09189	0.5	0	1
H120	H	0.17291	0.00801	0.5	0	1
H122	H	0.85472	0.33413	0.5	0	1
H123	H	0.92179	0.31749	0.5	0	1
H124	H	1.00601	0.38426	0.5	0	1

Table S3. Atomistic coordinates for the AA-stacking mode of **DICPO-COF** optimized using DFTB+ method. Space group: P6; α = β = 90°, γ = 120°, a = 33.9273 Å, b = 33.8870 Å, c = 4.6811 Å.

H1	H	0.88701	1.31213	0.68133	0	1

H2	H	1.10226	1.48154	0.68111	0	1
H3	H	1.53949	1.62487	0.6811	0	1
H4	H	1.71062	1.57918	0.68119	0	1
H5	H	0.39708	0.9196	0.68111	0	1
H6	H	0.44341	1.13497	0.68133	0	1
O7	O	1.02447	1.42491	0.73203	0	1
O8	O	1.59578	1.60336	0.73197	0	1
O9	O	0.41842	0.99745	0.73203	0	1
C10	C	0.42787	0.66494	0.5	0	1
C11	C	0.42436	0.62152	0.5	0	1
C12	C	0.46289	0.61678	0.5	0	1
C13	C	0.50717	0.65461	0.5	0	1
C14	C	0.51127	0.69821	0.5	0	1
C15	C	0.47266	0.70306	0.5	0	1
N16	N	0.54453	0.64485	0.5	0	1
C17	C	0.5922	0.68065	0.5	0	1
C18	C	0.38579	0.67036	0.5	0	1
C19	C	0.34135	0.6321	0.5	0	1
C20	C	0.30174	0.63584	0.5	0	1
C21	C	0.30802	0.6803	0.5	0	1
C22	C	0.35146	0.72001	0.5	0	1
C23	C	0.38963	0.71381	0.5	0	1

C24	C	0.35694	0.7676	0.5	0	1
C25	C	0.25416	0.59364	0.5	0	1
C26	C	0.31891	0.77425	0.5	0	1
C27	C	0.32379	0.81778	0.5	0	1
C28	C	0.36735	0.85739	0.5	0	1
C29	C	0.40512	0.85098	0.5	0	1
C30	C	0.40034	0.80762	0.5	0	1
C31	C	0.24743	0.54884	0.5	0	1
C32	C	0.20391	0.51012	0.5	0	1
C33	C	0.1644	0.51408	0.5	0	1
C34	C	0.17089	0.55835	0.5	0	1
C35	C	0.21424	0.59702	0.5	0	1
N36	N	0.37712	0.9046	0.5	0	1
C37	C	0.34135	0.91641	0.5	0	1
N38	N	0.11722	0.47656	0.5	0	1
C39	C	0.10533	0.42887	0.5	0	1
C40	C	0.6301	0.66944	0.5	0	1
N41	N	0.62116	0.62481	0.5	0	1
C42	C	0.66043	0.61799	0.5	0	1
C43	C	0.70488	0.6554	0.5	0	1
C44	C	0.71194	0.69918	0.5	0	1
C45	C	0.67525	0.70629	0.5	0	1

C46	C	0.65282	0.57043	0.5	0	1
N47	N	0.69124	0.56268	0.5	0	1
C48	C	0.68553	0.51699	0.5	0	1
C49	C	0.72553	0.51444	0.5	0	1
C50	C	0.72457	0.47279	0.5	0	1
C51	C	0.68299	0.43072	0.5	0	1
C52	C	0.64269	0.43351	0.5	0	1
C53	C	0.64376	0.47532	0.5	0	1
C54	C	0.68166	0.38498	0.5	0	1
C55	C	0.72204	0.38261	0.5	0	1
C56	C	0.72205	0.34095	0.5	0	1
C57	C	0.67922	0.30048	0.5	0	1
C58	C	0.63756	0.30038	0.5	0	1
C59	C	0.64002	0.34322	0.5	0	1
C60	C	0.76644	0.3397	0.5	0	1
C61	C	0.7668	0.2981	0.5	0	1
C62	C	0.80744	0.29717	0.5	0	1
C63	C	0.8501	0.33724	0.5	0	1
C64	C	0.85036	0.37905	0.5	0	1
C65	C	0.80964	0.38008	0.5	0	1
C66	C	0.59181	0.25588	0.5	0	1
C67	C	0.58889	0.21267	0.5	0	1

C68	C	0.54705	0.17186	0.5	0	1
C69	C	0.50551	0.17203	0.5	0	1
C70	C	0.5082	0.21469	0.5	0	1
C71	C	0.54986	0.25543	0.5	0	1
N72	N	0.4598	0.13201	0.5	0	1
N73	N	0.89001	0.33153	0.5	0	1
C74	C	0.93633	0.36996	0.5	0	1
C75	C	0.97633	0.36223	0.5	0	1
C76	C	0.45181	0.08567	0.5	0	1
C77	C	0.404	0.04556	0.5	0	1
C78	C	0.36712	0.05358	0.5	0	1
C79	C	0.32305	0.01749	0.5	0	1
C80	C	0.31552	0.02642	0.5	0	1
C81	C	0.35247	0.03441	0.5	0	1
N82	N	0.39714	0.00159	0.5	0	1
C83	C	0.96823	0.31723	0.5	0	1
C84	C	1.00423	0.30923	0.5	0	1
C85	C	1.04811	0.34569	0.5	0	1
C86	C	1.05618	0.39073	0.5	0	1
N87	N	1.02028	0.39943	0.5	0	1
H88	H	0.39241	0.59	0.5	0	1
H89	H	0.45818	0.58269	0.5	0	1

H90	H	0.54307	0.7297	0.5	0	1
H91	H	0.47965	0.7377	0.5	0	1
O92	O	0.60293	0.7207	0.5	0	1
H93	H	0.33757	0.59912	0.5	0	1
H94	H	0.27882	0.684	0.5	0	1
H95	H	0.42261	0.74308	0.5	0	1
H96	H	0.28429	0.74653	0.5	0	1
H97	H	0.29234	0.81803	0.5	0	1
H98	H	0.43917	0.88044	0.5	0	1
H99	H	0.43179	0.8072	0.5	0	1
H100	H	0.27507	0.54193	0.5	0	1
H101	H	0.2036	0.47835	0.5	0	1
H102	H	0.14151	0.56296	0.5	0	1
H103	H	0.21472	0.62897	0.5	0	1
O104	O	0.30136	0.88696	0.5	0	1
O105	O	0.13469	0.41831	0.5	0	1
H106	H	0.73446	0.65126	0.5	0	1
H107	H	0.74632	0.72803	0.5	0	1
H108	H	0.68244	0.74124	0.5	0	1
O109	O	0.61371	0.53903	0.5	0	1
H110	H	0.75832	0.54561	0.5	0	1
H111	H	0.75742	0.4753	0.5	0	1

H112	H	0.60914	0.40396	0.5	0	1
H113	H	0.61096	0.47271	0.5	0	1
H114	H	0.75374	0.41349	0.5	0	1
H115	H	0.6783	0.26877	0.5	0	1
H116	H	0.60922	0.34405	0.5	0	1
H117	H	0.73638	0.26518	0.5	0	1
H118	H	0.80571	0.26436	0.5	0	1
H119	H	0.88066	0.4119	0.5	0	1
H120	H	0.81374	0.41365	0.5	0	1
H121	H	0.61835	0.20864	0.5	0	1
H122	H	0.54954	0.14156	0.5	0	1
H123	H	0.47712	0.21636	0.5	0	1
H124	H	0.54743	0.28585	0.5	0	1
O125	O	0.94413	0.4091	0.5	0	1
O126	O	0.48313	0.07794	0.5	0	1
H127	H	0.37193	0.08761	0.5	0	1
H128	H	0.29461	0.02355	0.5	0	1
H129	H	0.28059	-0.05423	0.5	0	1
H130	H	0.93422	0.28796	0.5	0	1
H131	H	0.9981	0.27465	0.5	0	1
H132	H	1.07584	0.33855	0.5	0	1

Section E. NMR Spectra

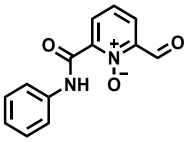

2-formyl-6-(phenylcarbamoyl)pyridine 1-oxide: brown solid; 62% yield;**^{1}H NMR (400 MHz, CDCl$_3$)** δ 10.18 (s, 1H), 9.93 (s, 1H), 8.56 (dd, *J* = 7.0, 1.8 Hz, 1H), 8.17 – 8.12 (m, 2H), 7.81 (d, *J* = 7.8 Hz, 2H), 7.42 (t, *J* = 7.9 Hz, 2H), 7.19 (d, *J* = 7.5 Hz, 1H). **^{13}C NMR (100 MHz, CDCl$_3$)** δ 192.09, 160.89, 139.11, 137.32, 130.28, 129.22, 126.68, 124.82, 124.10, 119.93. **HRMS m/z (ESI)** calcd for C13H11N2O3+ (M + H) + 243.0764, found 243.0757.

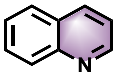

quinoline[2]: Yellow oil; 85% yield; **^{1}H NMR (400 MHz, CDCl$_3$)** δ 8.88 – 8.82 (m, 1H), 8.05 (dd, *J* = 20.2, 8.4 Hz, 2H), 7.71 (d, *J* = 8.2 Hz, 1H), 7.64 (t, *J* = 7.4 Hz, 1H), 7.45 (t, *J* = 7.5 Hz, 1H), 7.28 (dd, *J* = 8.3, 4.2 Hz, 1H).0

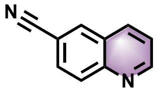

quinoline-6-carbonitrile[3]: Yellow solid; 80% yield; **^{1}H NMR (400 MHz, CDCl$_3$)** δ 9.07 (s, 1H), 8.27 – 8.16 (m, 3H), 7.87 (dd, *J* = 8.7, 1.7 Hz, 1H), 7.55 (dd, *J* = 8.3, 4.1 Hz, 1H).

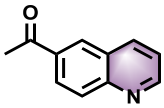

methyl quinoline-6-carboxylate[4]: White solid; 82% yield; **^{1}H NMR (400 MHz, CDCl$_3$)** δ 9.03 – 8.96 (m, 1H), 8.59 (d, *J* = 1.8 Hz, 1H), 8.28 (ddd, *J* = 16.6, 8.6, 1.5 Hz, 2H), 8.14 (d, *J* = 8.8 Hz, 1H), 7.47 (dd, *J* = 8.3, 4.2 Hz, 1H), 3.99 (s, 3H).

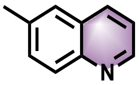

6-methylquinoline[4]: Colorless liquid; 55% yield; **^{1}H NMR (400 MHz, CDCl$_3$)** δ 7.97 (s, 1H), 7.42 (s, 1H), 7.24 (t, *J* = 9.0 Hz, 1H), 7.12 (t, *J* = 2.7 Hz, 1H), 7.01 (d, *J* = 8.2 Hz, 1H), 6.45 (s, 1H), 2.44 (s, 3H).

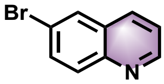

6-bromoquinoline[4]: Yellow solid; 80% yield; **^{1}H NMR (400 MHz, CDCl$_3$)** δ 8.92 (dd, *J* = 4.1, 1.5 Hz, 1H), 8.10 – 8.04 (m, 1H), 7.99 – 7.94 (m, 2H), 7.78 (dd, *J* = 9.0, 2.1 Hz, 1H), 7.42 (dd, *J* = 8.3, 4.2 Hz, 1H).

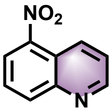

5-nitroquinoline: Brown solid; 65% yield; **^{1}H NMR (400 MHz, CDCl$_3$)** δ 9.06 (dd, *J* = 4.2, 1.7 Hz, 1H), 8.26 (dd, *J* = 8.4, 1.7 Hz, 1H), 8.03 (d, *J* = 7.9 Hz, 2H), 7.61 (t, *J* = 7.9 Hz, 1H), 7.55 (dd, *J* = 8.4, 4.2 Hz, 1H).

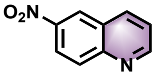

6-nitroquinoline[4]: Yellow amorphous solid; 67% yield; **^{1}H NMR (400 MHz, CDCl$_3$)** δ 9.18 – 8.99 (m, 2H), 8.38 – 8.24 (m, 2H), 7.99 (d, *J* = 9.0 Hz, 1H), 7.60 (dd, *J* = 8.4, 4.1 Hz, 1H).

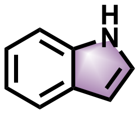

1H-indole[2]: Beige solid; 60% yield; **^{1}H NMR (400 MHz, CDCl$_3$)** δ 8.03 (s, 1H), 7.65 (d, *J* = 7.9 Hz, 1H), 7.38 – 7.34 (m, 1H), 7.22 – 7.17 (m, 1H), 7.17 – 7.14 (m, 1H), 7.14 – 7.09 (m, 1H), 6.57 – 6.50 (m, 1H).

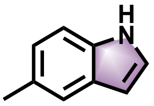

5-methyl-1H-indole[4]: White solid; 55% yield; **^{1}H NMR (400 MHz, $CDCl_3$)** δ 7.50 (d, *J* = 7.2 Hz, 2H), 7.15 (d, *J* = 7.8 Hz, 1H), 7.07 (pd, *J* = 7.0, 1.3 Hz, 2H), 6.17 (s, 1H), 2.31 (s, 3H).

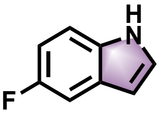

5-fluoro-1H-indole[5]: White solid; 52% yield; **^{1}H NMR (400 MHz, $CDCl_3$)** δ 8.15 (s, 1H), 7.30 (td, *J* = 9.0, 3.4 Hz, 2H), 7.25 (d, *J* = 2.8 Hz, 1H), 6.95 (td, *J* = 9.1, 2.5 Hz, 1H), 6.52 (s, 1H).

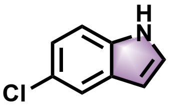

5-chloro-1H-indole[5]: Pale yellow solid; 53% yield; **^{1}H NMR (400 MHz, $CDCl_3$)** δ 8.18 (s, 1H), 7.61 (d, *J* = 2.0 Hz, 1H), 7.31 (d, *J* = 8.6 Hz, 1H), 7.23 (t, *J* = 2.8 Hz, 1H), 7.15 (dd, *J* = 8.6, 2.0 Hz, 1H), 6.50 (t, *J* = 2.7 Hz, 1H).

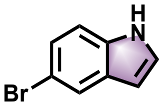

5-bromo-1H-indole[5]: Brown solid; 55% yield; **^{1}H NMR (400 MHz, $CDCl_3$)** δ 8.17 (s, 1H), 7.76 (s, 1H), 7.25 (d, *J* = 6.0 Hz, 2H), 7.22 – 7.18 (m, 1H), 6.57 – 6.24 (m, 1H).

Section F. Copies of NMR Spectra

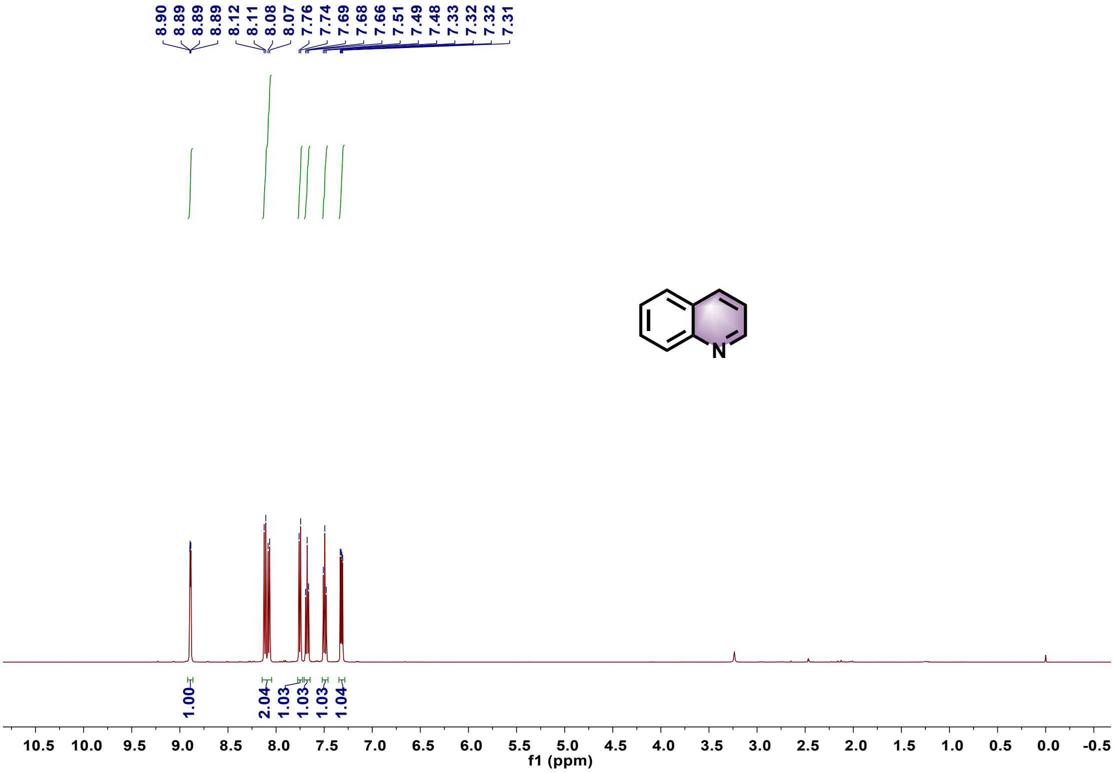

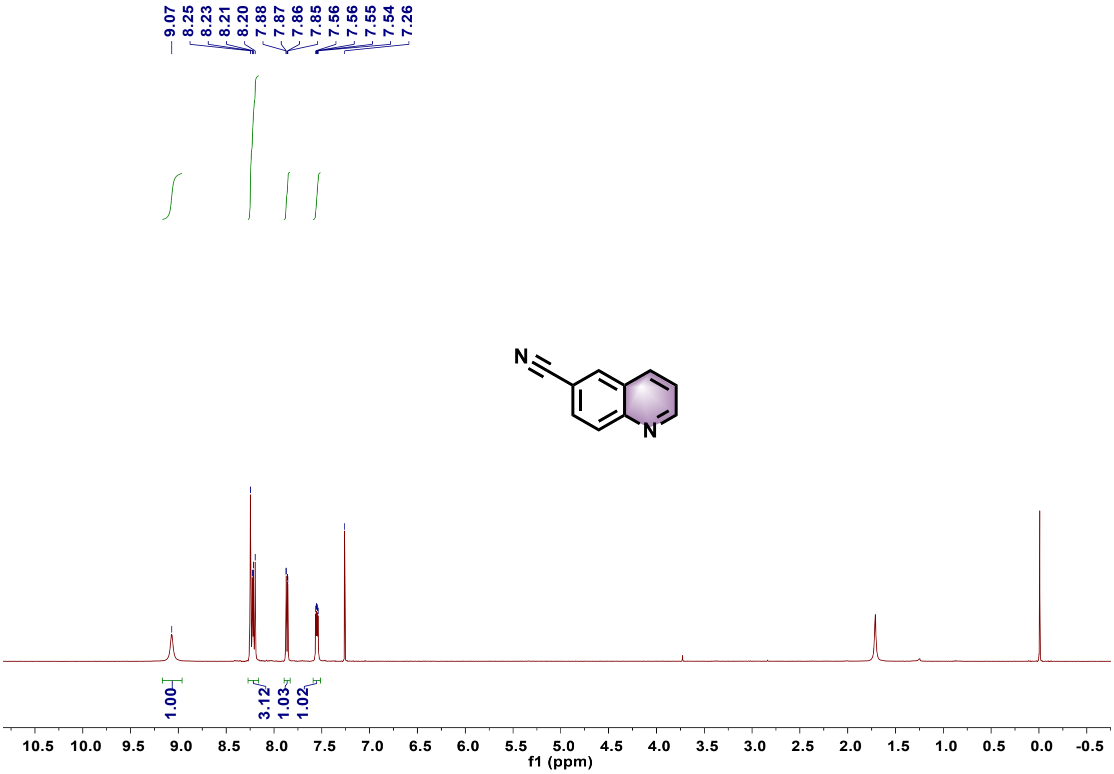

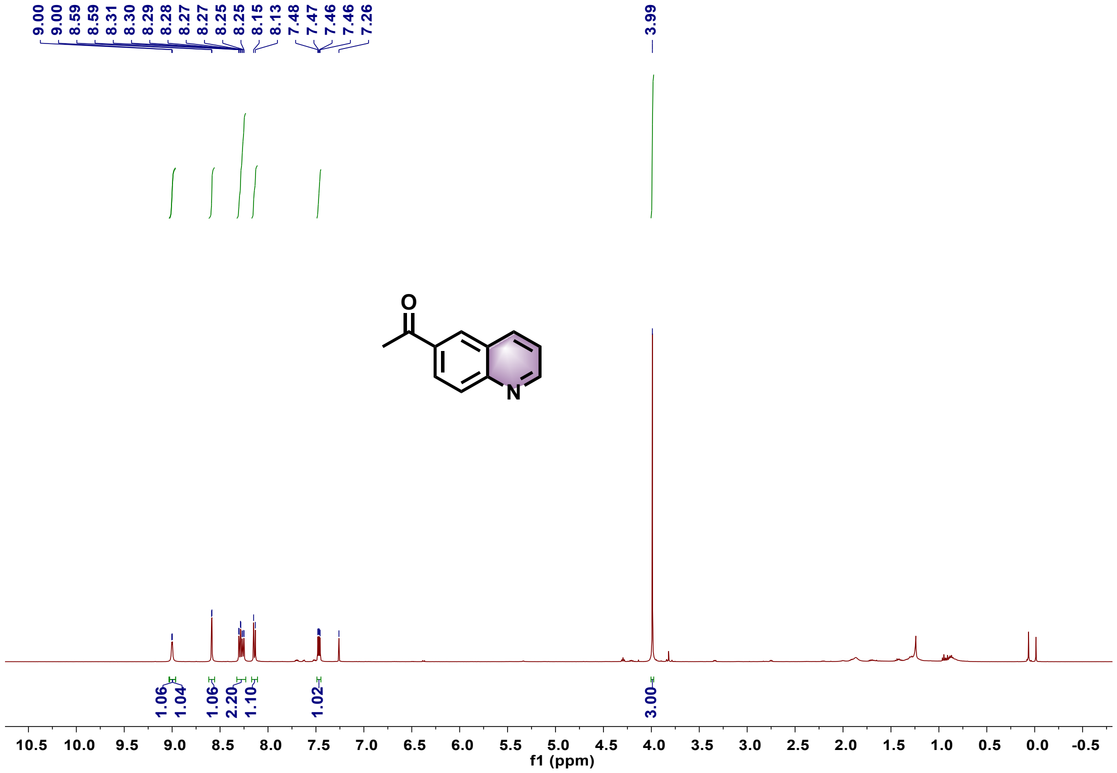
9.00
9.00
8.59
8.59
8.31
8.30
8.29
8.28
8.27
8.27
8.25
8.25
8.15
8.13
7.48
7.47
7.46
7.46
7.26
3.99
O
N
1.06
1.04
1.06
2.20
1.10
1.02
3.00
10.5
10.0
9.5
9.0
8.5
8.0
7.5
7.0
6.5
6.0
5.5
5.0
4.5
4.0
3.5
3.0
2.5
2.0
1.5
1.0
0.5
0.0
-0.5
f1 (ppm)

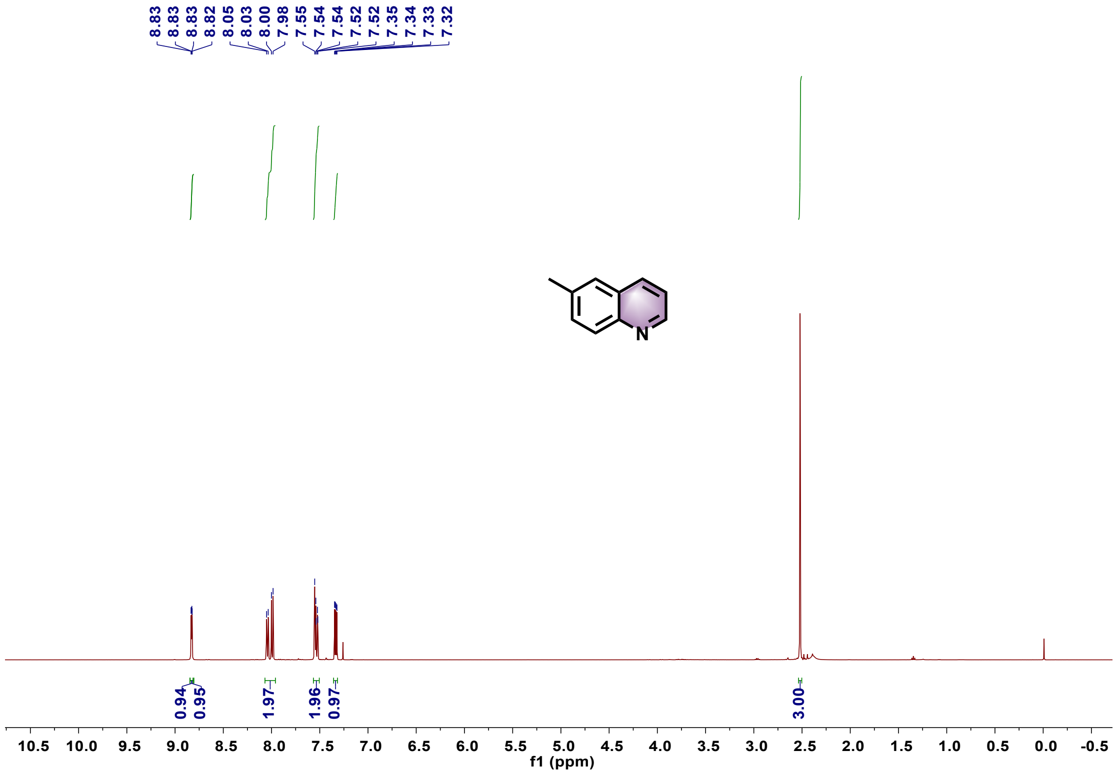
8.83
8.83
8.83
8.82
8.05
8.03
8.00
7.98
7.55
7.54
7.54
7.52
7.52
7.35
7.34
7.33
7.32
N
0.94
0.95
1.97
1.96
0.97
3.00
10.5
10.0
9.5
9.0
8.5
8.0
7.5
7.0
6.5
6.0
5.5
5.0
4.5
4.0
3.5
3.0
2.5
2.0
1.5
1.0
0.5
0.0
-0.5
f1 (ppm)

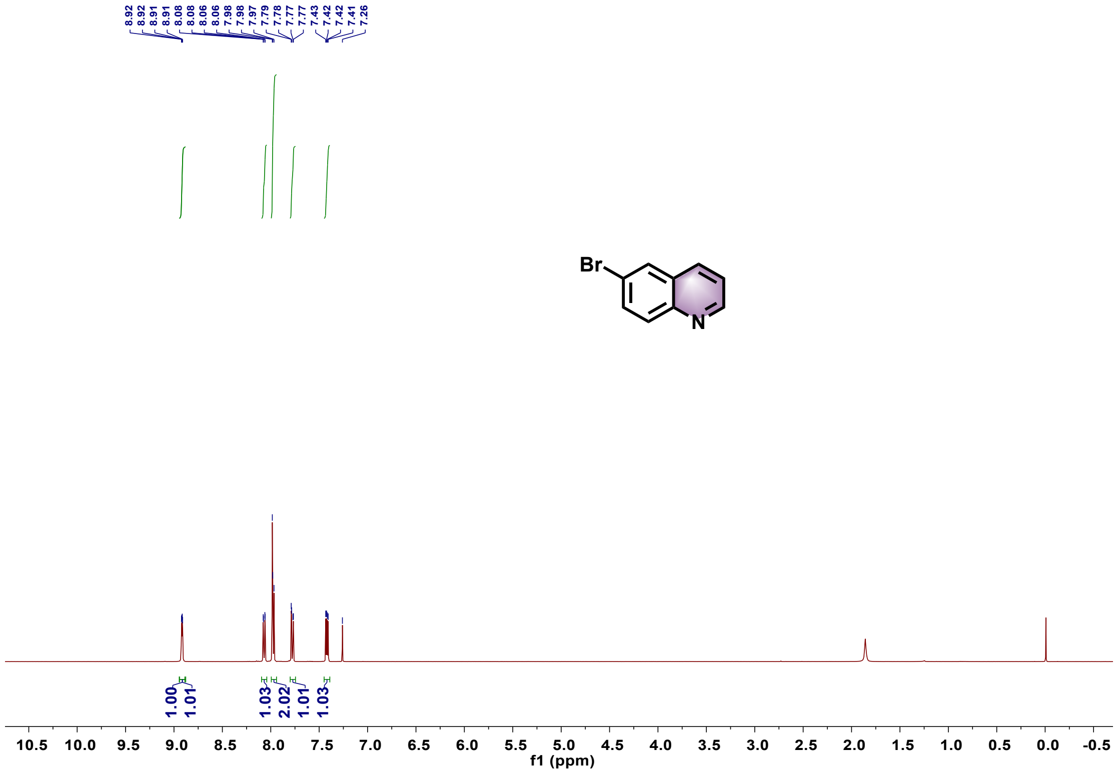
8.92
8.92
8.91
8.91
8.08
8.08
8.06
8.06
7.98
7.98
7.97
7.79
7.78
7.77
7.77
7.43
7.42
7.42
7.41
7.26
Br
N
1.00
1.01
1.03
2.02
1.01
1.03
10.5
10.0
9.5
9.0
8.5
8.0
7.5
7.0
6.5
6.0
5.5
5.0
4.5
4.0
3.5
3.0
2.5
2.0
1.5
1.0
0.5
0.0
-0.5
f1 (ppm)

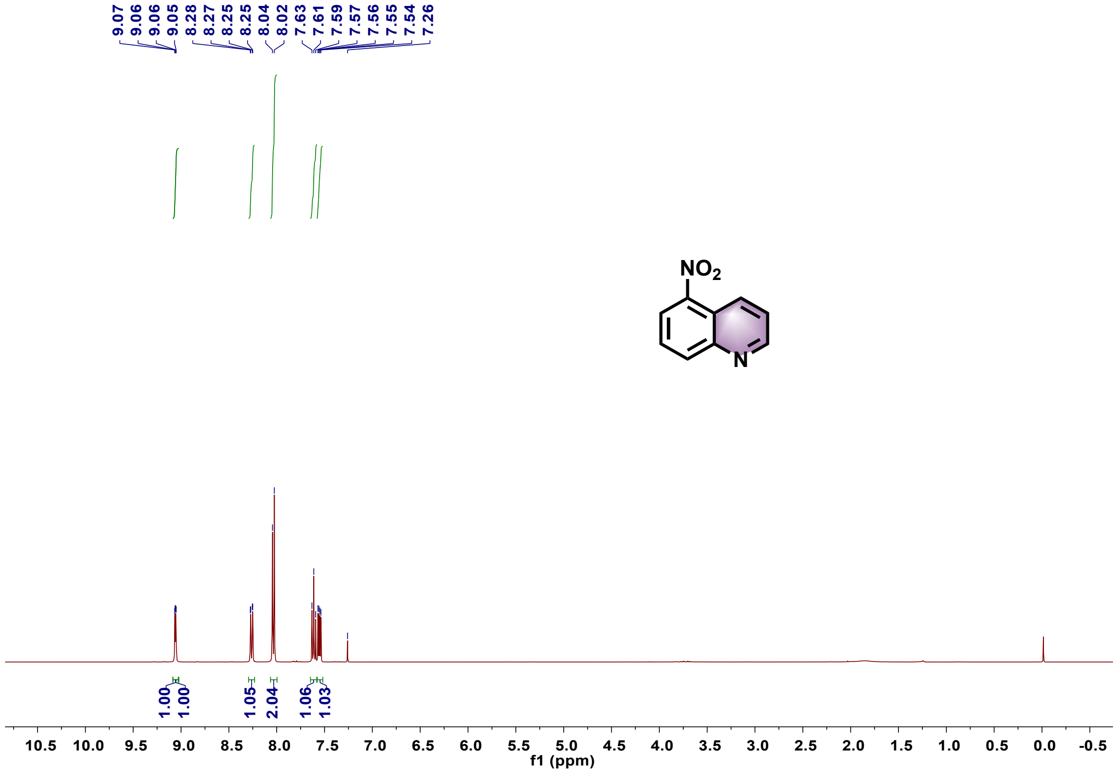
9.07
9.06
9.06
9.05
8.28
8.27
8.25
8.25
8.04
8.02
7.63
7.61
7.59
7.57
7.56
7.55
7.54
7.26
NO2
N
1.00
1.00
1.05
2.04
1.06
1.03
10.5
10.0
9.5
9.0
8.5
8.0
7.5
7.0
6.5
6.0
5.5
5.0
4.5
4.0
3.5
3.0
2.5
2.0
1.5
1.0
0.5
0.0
-0.5
f1 (ppm)

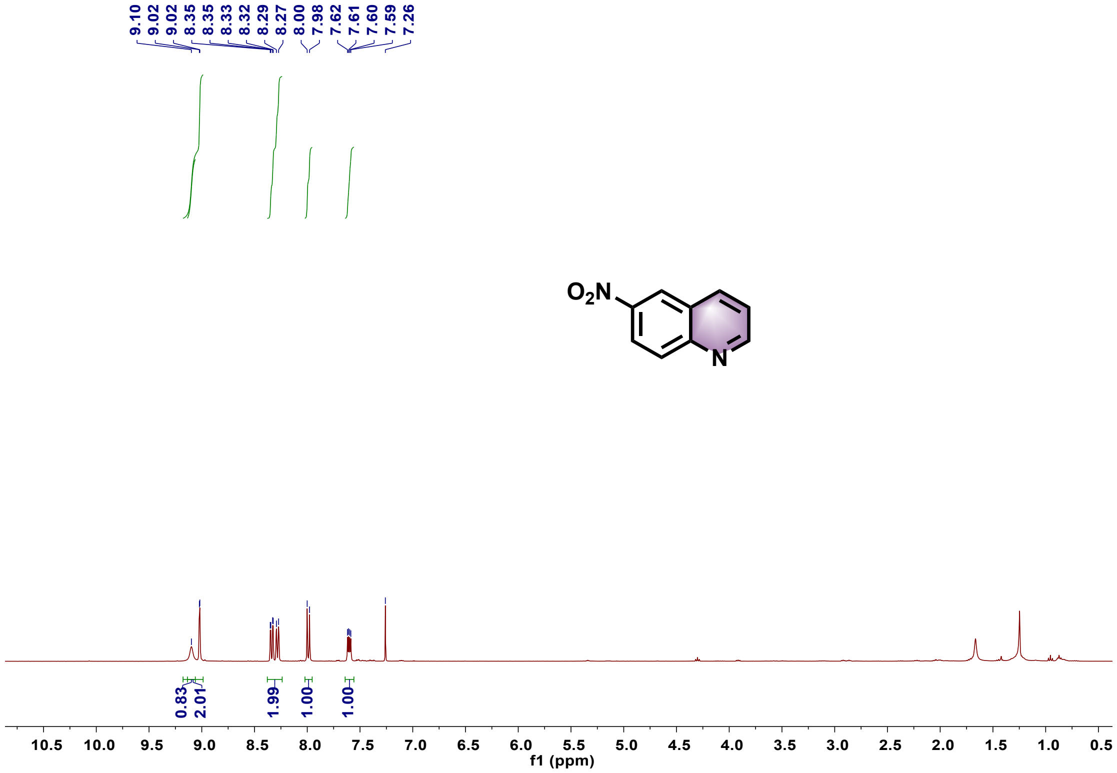
9.10
9.02
9.02
8.35
8.35
8.33
8.32
8.29
8.27
8.00
7.98
7.62
7.61
7.60
7.59
7.26
O_2N
N
0.83
2.01
1.99
1.00
1.00
10.5
10.0
9.5
9.0
8.5
8.0
7.5
7.0
6.5
6.0
5.5
5.0
4.5
4.0
3.5
3.0
2.5
2.0
1.5
1.0
0.5
f1 (ppm)

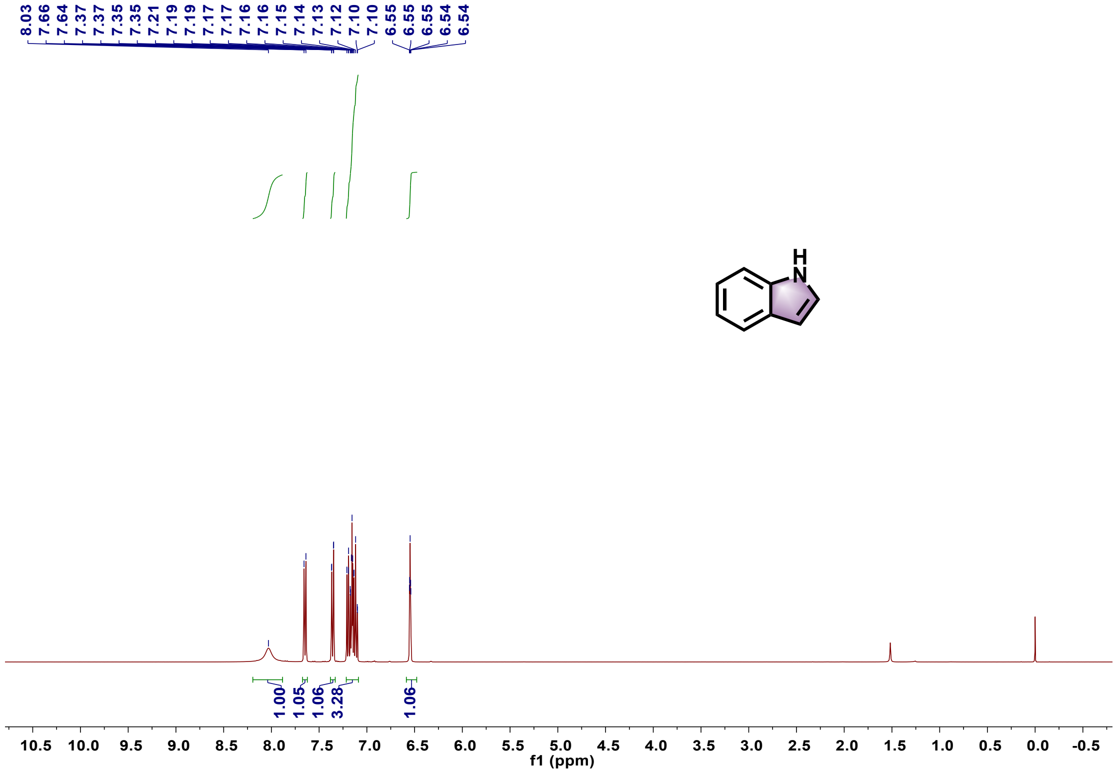
8.03
7.66
7.64
7.37
7.37
7.35
7.35
7.21
7.19
7.19
7.17
7.17
7.16
7.16
7.15
7.14
7.13
7.12
7.10
6.55
6.55
6.55
6.54
6.54
H
N
1.00
1.05
1.06
3.28
1.06
10.5
10.0
9.5
9.0
8.5
8.0
7.5
7.0
6.5
6.0
5.5
5.0
4.5
4.0
3.5
3.0
2.5
2.0
1.5
1.0
0.5
0.0
-0.5
f1 (ppm)

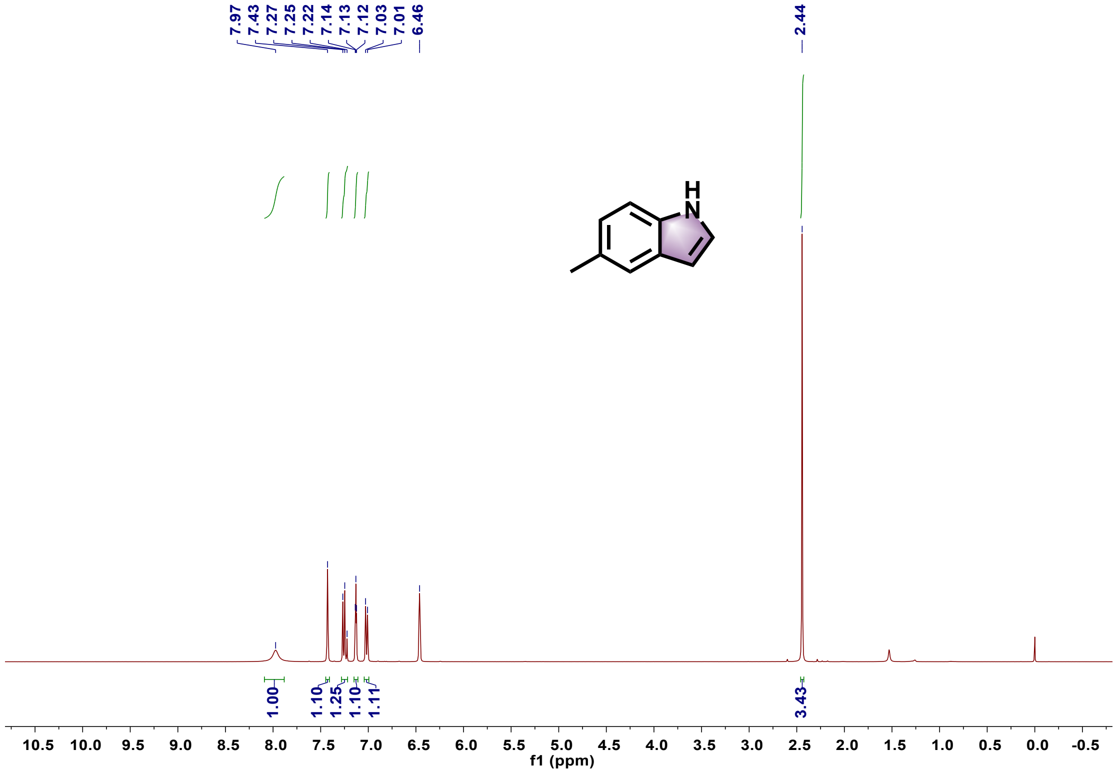
7.97
7.43
7.27
7.25
7.22
7.14
7.13
7.12
7.03
7.01
6.46
2.44
H
N
1.00
1.10
1.25
1.10
1.11
3.43
10.5
10.0
9.5
9.0
8.5
8.0
7.5
7.0
6.5
6.0
5.5
5.0
4.5
4.0
3.5
3.0
2.5
2.0
1.5
1.0
0.5
0.0
-0.5
f1 (ppm)

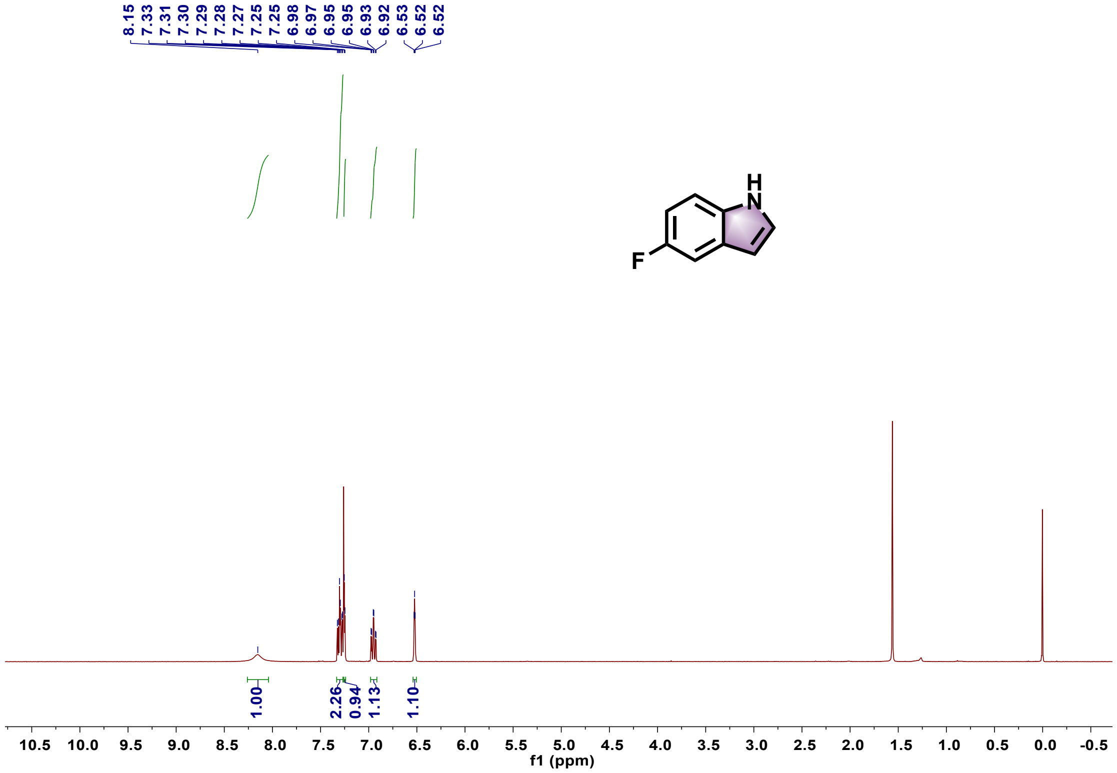
8.15
7.33
7.31
7.30
7.29
7.28
7.27
7.25
7.25
6.98
6.97
6.95
6.95
6.93
6.92
6.53
6.52
6.52
H
N
F
1.00
2.26
0.94
1.13
1.10
10.5
10.0
9.5
9.0
8.5
8.0
7.5
7.0
6.5
6.0
5.5
5.0
4.5
4.0
3.5
3.0
2.5
2.0
1.5
1.0
0.5
0.0
-0.5
f1 (ppm)

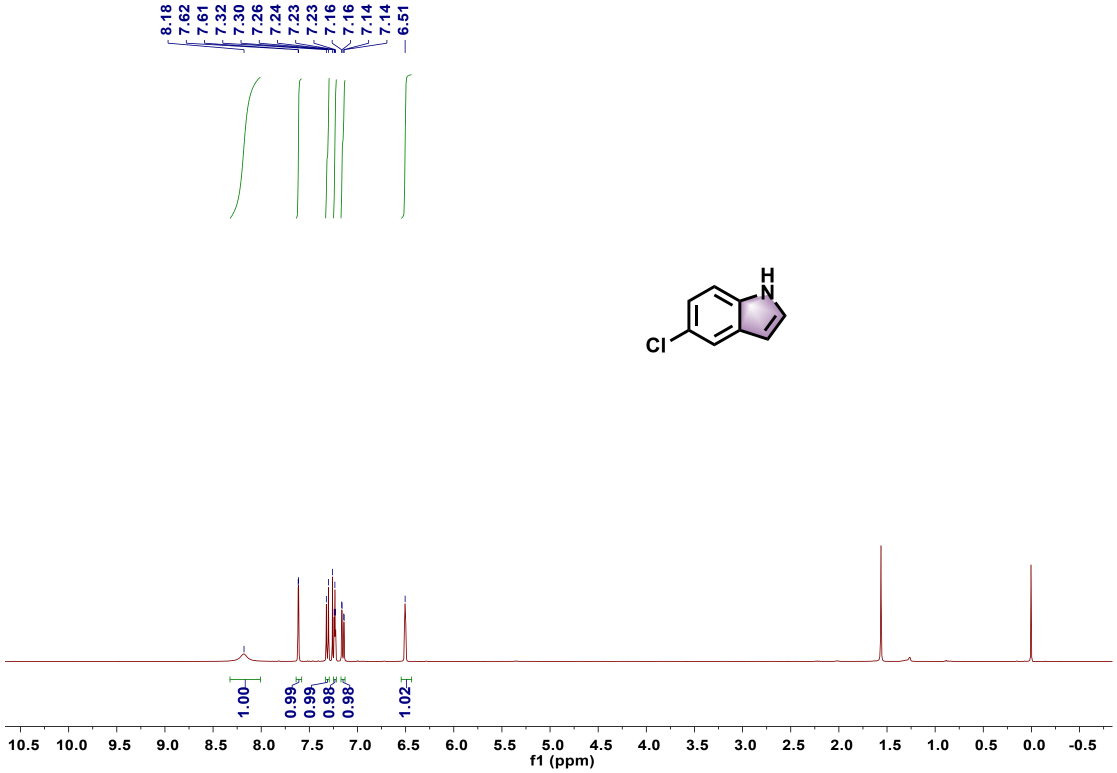
8.18
7.62
7.61
7.32
7.30
7.26
7.24
7.23
7.23
7.16
7.16
7.14
7.14
6.51
H
N
Cl
1.00
0.99
0.99
0.98
0.98
1.02
10.5
10.0
9.5
9.0
8.5
8.0
7.5
7.0
6.5
6.0
5.5
5.0
4.5
4.0
3.5
3.0
2.5
2.0
1.5
1.0
0.5
0.0
-0.5
f1 (ppm)

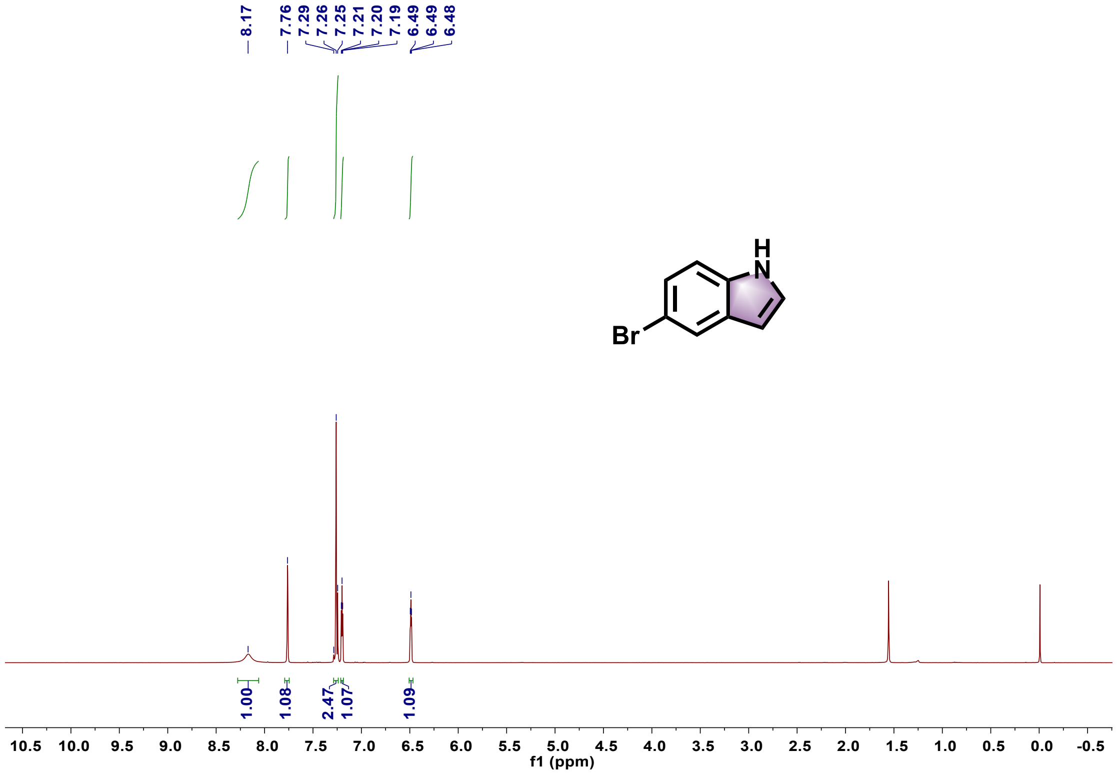
8.17
7.76
7.29
7.26
7.25
7.21
7.20
7.19
6.49
6.49
6.48
H
N
Br
1.00
1.08
2.47
1.07
1.09
10.5
10.0
9.5
9.0
8.5
8.0
7.5
7.0
6.5
6.0
5.5
5.0
4.5
4.0
3.5
3.0
2.5
2.0
1.5
1.0
0.5
0.0
-0.5
f1 (ppm)

Section G. Supporting References

S1. Ferrarini, A.; Soek, R. N.; Rebecchi Rios, R.; Santana, F. S.; Campos, R. B.; da Silva, R. S.; Nunes, F. S., Structural, spectral, and photoreactivity properties of mono and polymetallated-2,2′-bipyridine ruthenium(II) complexes. *Inorg. Chim. Acta.* **2022,** *533* (1), 120771-120785.

S2. Konev, M. O.; Cardinale, L.; Jacobi von Wangelin, A., Catalyst-Free N-Deoxygenation by Photoexcitation of Hantzsch Ester. *Org. Lett.* **2020,** *22* (4), 1316-1320.

S3. Bone, K. I.; Puleo, T. R.; Bandar, J. S., Direct C–H Hydroxylation of N-Heteroarenes and Benzenes via Base-Catalyzed Halogen Transfer. *J. Am. Chem. Soc* **2024,** *146* (14), 9755-9767.

S4. Pathania, V.; Roy, S. R., Phenalenyl-Based Photocatalyst for Bioinspired Oxidative Dehydrogenation of N-Heterocycles and Benzyl Alcohols. *J. Org. Chem.* **2024,** *89* (6), 4145-4155.

S5. Zhang, T.; Lv, Y.; Zhang, Z.; Jia, Z.; Loh, T.-P., A Rare Earth Metal Catalyzed Aerobic Dehydrogenation of N-Heterocycles. *Org. Lett.* **2023,** *25* (24), 4468-4472.